Frontiers in Bioscience Landmark

Front. Biosci. (Landmark Ed) **2023**; 28(5): 94
https://doi.org/10.31083/j.fbl2805094

Original Research

The Cardioprotective Effects and Mechanisms of Astragalus-Safflower Herb Pairs on Coronary Heart Disease Identified by Network Pharmacology and Experimental Verification

Yong Yuan[1,2,†], Huajiang Liu[3,†], Qingwen Meng[4,5,*]

[1]College of Pediatrics, Hainan Medical University, 571199 Haikou, Hainan, China
[2]Department of Traditional Chinese Medicine, The First Affiliated Hospital of Hainan Medical University, 570100 Haikou, Hainan, China
[3]Department of Interventional Vascular Surgery, The First Affiliated Hospital of Hainan Medical University, 570100 Haikou, Hainan, China
[4]Hainan Provincial Key Laboratory of Tropical Brain Research and Transformation, Hainan Medical University, 571199 Haikou, Hainan, China
[5]Department of Cardiovascular Medicine, The First Affiliated Hospital of Hainan Medical University, 570100 Haikou, Hainan, China
*Correspondence: mengqingwen66@hainmc.edu.cn (Qingwen Meng)
[†]These authors contributed equally.

Academic Editor: Marcello Iriti
Submitted: 19 December 2022 Revised: 6 February 2023 Accepted: 10 February 2023 Published: 22 May 2023

Abstract

Background: Huang Qi (HQ, Astragalus) and Hong Hua (HH, Safflower), two Chinese herbal remedies, are widely used to treat coronary heart disease (CHD). However, the underlying mechanisms of this herb pair remain unclear. The aim of this study was to determine the potential synergistic effects and mechanisms of Astragalus-Safflower in the treatment of CHD. **Methods**: Network pharamcology was performed to identify the core components, targets, and key genes of Astragalus-Safflower herbal pair (ASHP) for the treatment of CHD. Enrichment analysis was performed to identify overlapping genes. Ultrahigh-performance liquid chromatography coupled with Q-Exactive MS/MS (UHPLC-QE-MS) was used to detect the blood component of rat ASHP drug-containing serum, which is also considered to be the core components of the ASHP. Molecular docking of ASHP core compounds with core proteins of the pyroptosis pathway mediated by the NLR family pyrin domain containing 3 (NLRP3) inflammasomes. *In vivo* experiments were conducted to verify the effect and mechanism of ASHP in the CHD mice model. **Results**: 54 active compounds and 404 target genes were identified from ASHP, and 1576 targets for CHD with 90 overlapping genes for both. *IL6, AKT1, IL1B, TP53, VEGFA, PTGS2, MMP9, CCL2, CXCL8* and *EGF* were the key hub target genes. Enrichment analysis of Kyoto Encyclopedia of Gene and Genome (KEGG) revealed that the NLRP3 inflammasome-mediated signaling pathway was one of the more critical signaling pathways. The UHPLC-QE-MS was used to identify the rat ASHP containing serum enrollment compound as calycosin and isorhamnetin. Molecular docking showed that quercetin, kaempferol, apigenin, calycosin and isorhamnetin possessed good binding sites with NLRP3 and Caspase-1. Animal experiments showed that the expression of NLRP3, Caspase-1, GSDMD, IL-1β mRNA and protein levels were elevated in mouse models of CHD, and decreased after intervention with ASHP. **Conclusions**: ASHP can effectively treat CHD, and the mechanism may be related to the inhibition of the NLRP3 inflammasome-mediated pathway.

Keywords: coronary heart disease; Astragalus-Safflower herb pair; network pharmacology; NLRP3 inflammasome; pyroptosis

1. Introduction

Cardiovascular disease (CVD) accounts for about one-third of all deaths worldwide each year. The number of CVD cases worldwide reached 523 million in 2019 and 18.6 million CVD deaths by 2019 [1]. According to a recent report released by the National Center for CVD, the number of people with CVD in China is about 330 million, including 11 million with coronary heart disease (CHD) [2]. Myocardial ischemia, hypoxia, or necrosis is caused by stenosis of the coronary arteries or obstruction by atherosclerosis (AS), resulting in CHD. Drug therapy is one of the most basic treatments for CHD, and commonly used drugs include anti-thrombotic drugs, lipid-lowering drugs, β-blockers, calcium channel blockers, and renin-angiotensin system inhibitors, but most drugs act on a single target and long-term use of these drugs is often associated with adverse effects such as liver function impairment, bradycardia and hemorrhage [3–5]. Therefore, there is an urgent need to develop drugs with multiple active ingredients and multiple therapeutic targets.

Traditional Chinese medicine (TCM) has long been used in China for the treatment of CHD due to multi-target and multi-component advantages [6]. According to the TCM theory, the primary cause of CHD is qi deficiency and blood stasis, and therefore reviving qi and fostering blood circulation are the primary principles in the treatment of CHD [7]. Astragalus and Safflower are representative herbal medicines for reviving qi and fostering blood circulation [8]. Astragalus is the root of the leguminous plant *Astragalus membranaceus*, family legume, which has the effects of invigorating qi, eliminating toxins, draining diuresis, regenerating muscles, and strengthening body re-

sistance. Astragalus has been shown to play a protective role in ischemic stroke, improvement of myocardial fibrosis and myocardial remodeling, lung injury and other diseases [9]. The primary active ingredient of the plant Astragalus membranaceus is Astragaloside IV (AGIV). A study reported that astragaloside IV enhanced the vasodilatation function in rat aorta endothelial cells (ECs) by controlling the PI3K/Akt/eNOS signaling pathway [10]. Formononetin is an isoflavone extracted from Astragalus membranaceus. It can substantially attenuate the development of atherosclerosis by regulating the interplay between krüppel-like factor 4(KLF4) and Scavenger receptor A (SRA), suggesting that formononetin might be a novel therapeutic approach for inhibiting atherosclerosis [11]. By triggering ROS/NLRP3-mediated suppression of the inflammatory response, AS-IV prevented pyroptosis in human umbilical vein endothelial cells (HUVECs) that had been triggered by lipopolysaccharide (LPS) [12]. Safflower is the flower of the *Carthamus tinctorius* L., family Asteraceae, which has the properties of activating blood circulation, dispersing blood stasis, and relieving pain. Our previous study showed that Safflower could exert anti-apoptotic effects by regulating the expression of proteins related to Bax, Bcl-2 and SIRT1/FoxO1 signaling pathways for the treatment of CAD [13]. Hydroxy saffron yellow A (HSYA) is one of the main components of Safflower. A study by Qiang Xu *et al*. [14] showed that through inflammation, Bcl-2/Bax and the PPAR signaling pathway, HSYA could attenuate the symptoms of CAD. In recent years, more and more studies have shown that Safflower has shown effective protective effects in diseases such as atherosclerosis and myocardial ischemia-reperfusion(I/R) injury [13,15]. The main active components of Safflower has been shown to suppress foam cell formation, vascular smooth muscle cell proliferation and migration, and platelet activation [16]. In summary, Astragalus and Safflower can promote blood flow, prevent thrombosis, and removing congestion. The use of ASHP has been studied in ischemic stroke and cerebral I/R injury [8,17]. Chen *et al*. [18] have demonstrated the preventive benefits of combination use of their two active ingredients calycosin and hydroxysafflor yellow A against cerebral I/R injury in a rat model. However, the effects and mechanisms of ASHP in the prevention and treatment of CHD are unclear.

Network pharmacology can rigorously assess the relationships between illnesses and medications and pinpoint the precise processes by which each drug acts on the genes it is designed to target [19]. This study was intended to clarify the specific components and targets of the action of ASHP, explore its underlying mechanism in CHD through network pharmacology and molecular docking, envisage the clinical application of ASHP in CHD. The general flowchart of the study is shown in Fig. 1.

2. Materials and Methods

2.1 Network Pharmacology

2.1.1 Active Ingredients and Target Prediction of ASHP

The traditional chinese medicine systems pharmacology database and analysis platform (TCMSP) database (https://old.tcmsp-e.com/tcmsp.php) was searched using the keywords "Astragalus and Safflower", and the active compounds were screened based on the oral bioavailability (OB) $\geq$30% and drug-likeness (DL) $\geq$0.18 of the monomers [19]. Screening of the potent compounds and their relative targets was performed by the STRING database (http://www.string-db.org) by setting the screening species category and transferring the target protein name to "gene symbol" [20].

2.1.2 Screening of CHD-Related Targets

Using the keyword "coronary heart disease" as a search term, we used the disease database (DisGeNET, http://www.disgenet.org) to find disease targets [21].

2.1.3 Prediction of Potential Targets of ASHP Against CHD

The main pharmacological targets of ASHP and the corresponding target genes of CHD were introduced into the online website bioinformatics (http://www.bioinformatics.com.cn) [22]. The overlap targets were the potential therapeutic target genes of ASHP for CHD.

2.1.4 Protein-Protein Interaction (PPI) Network Construction and Analysis

The obtained overlapping genes were imported into the STRING database, and the species "*homo sapiens*" was selected with the lowest interaction score of 0.40 at the highest confidence level to obtain the PPI network map of overlapping genes, which was then imported into Cytoscape (Version 3.8.0, Oracle, Austin, TX, USA) to obtain the most significant top 10 hub genes using the degree algorithm in the cytoHubba plug-in.

2.1.5 Construction of the "Compound-Target-Disease" Network

The active compounds of ASHP, CHD-related targets and overlapping genes were imported into Cytoscape to construct a network diagram to understand the correlation of the three more visually. The "Compound-Target-Disease" network was created using Cytoscape [23].

2.1.6 Gene Ontology (GO) Enrichment and Kyoto Encyclopedia of Gene and Genome (KEGG) Pathway Analysis

GO and KEGG enrichment analysis were performed on the key target genes screened by the Metascape database (https://metascape/org/gp) [24]. The search species was limited to *homo sapiens*, minimum overlap was set to 3, *p*-value cutoff was set to 0.01, and minimum enrichment

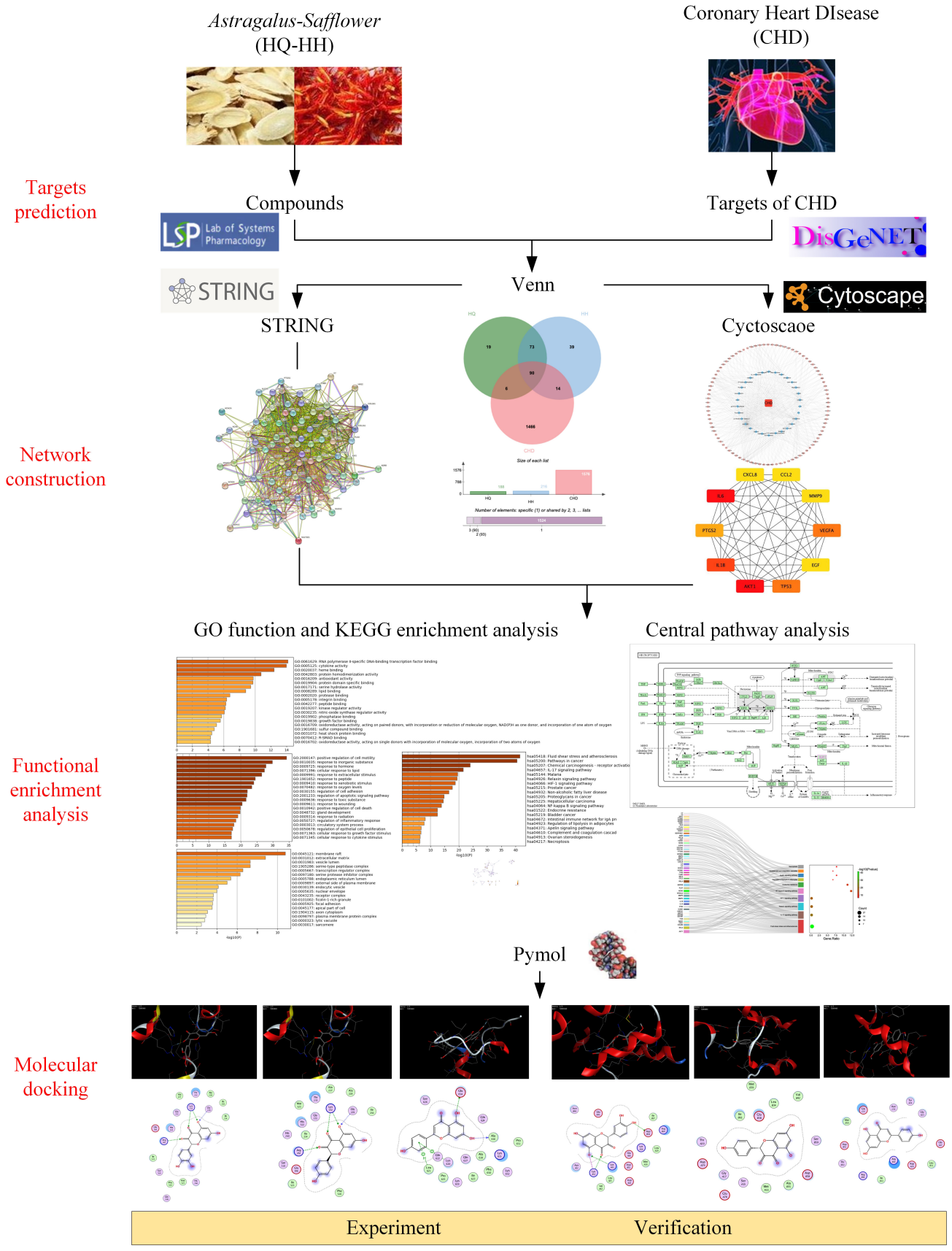

Fig. 1. The overall process of the study.

was set to 0.01. The GO and KEGG signaling pathways involved in the therapeutic effect of ASHP were obtained. Sankey dot plots were plotted by the online platform bioinformatics (https://www.bioinformatics.com.cn).

2.1.7 Molecular Docking

The pubchem database (https://pubchem.ncbi.nlm.nih.gov/) was searched for InChIKey numbers of drug small molecules and download 3D structures of drug small molecules [25]. The crystal structure of the core target protein was downloaded using the RCSB PDB database (http://www.rcsb.org/), and the water molecules and ligand small molecules were removed with PyMol software (Version 2.5, Schrodinger Inc., New York, NY, USA) to obtain the 3D structure of the receptor protein. MOE software (Version 2019.0102, Chemical Computing Group Inc., Montreal, Canada) was used to perform the fractionation of ligand small molecules and protein receptors. The docking of ligand small molecules and protein receptors was performed using MOE software. It is generally believed that either the conformation with a lower binding energy between molecules or the conformation with the lowest energy is more stable. In this study, the optimal conformation with the lowest energy was selected and the docking results were visualized by PyMol software.

2.2 Ultrahigh-Performance Liquid Chromatography Coupled with Q-Exactive MS/MS (UPLC-QE-MS/MS)

2.2.1 Preparation of Drug-Containing Serum

Ten SPF grade healthy male Sprague-Dawley (SD) rats (180 $\pm$ 20 g) were provided by Changsha Tianqin Biotechnology Co. Ltd. (License number: SCXK (xiang) 2019-0014, Changsha, China). All SD rats were provided food and drink freely, and kept at a temperature of 20–24 °C and the relative humidity of 50–70%. The Institutional Animal Care and Use Committee of Hainan Medical University approved all animal experimentation techniques (Number: HYLL-2021-140). The animal experiment followed Guidelines for Ethical Review of the Welfare of Laboratory Animals in the People's Republic of China [GB/T 35892-2018]. The rats were divided into two groups, the blank serum group (n = 5) and the Astragalus-Safflower drug-containing serum group (n = 5). ASHP granules were purchased from Guangdong YI Fang Chinese Medicine Granules Co. (Foshan, China). Astragalus-Safflower granules (Astragalus 3 g/kg, Safflower 1 g/kg) were given, and gastric gavage was continuously administered 7 times, and blood was taken from the abdominal aorta 1h after the last dose. Rats in the blank serum group were given an equal volume of normal saline for gavage. The supernatant was extracted, filtered, and inactivated in a water bath at 56 °C for 30 min, and the sera from the same group was mixed and stored at –20 °C [13].

2.2.2 Processing of Serum Samples

400 μL of plasma sample was combined with 40 μL of hydrochloric acid, which was then vortexed for 1 minute before being incubated at 4 °C for 15 minutes. then 1.6 mL of acetonitrile was added, vortex the mixture for 5 minutes, and then centrifuge the samples at 12000 rpm for 5 minutes at 4 °C. A new tube was filled with 1800 μL of supernatant, and it was nitrogen dried. The dried samples were reconstituted by vortexing for five minutes in 150 μL of 80% methyl alcohol containing 1 g/mL of internal standard. Then, the mixture was centrifuged at 12000 rpm for 5 minutes at 4 °C , and 120 μL of the supernatant was transferred to a new glass vial for liquid chromatography mass spectrometry(LC/MS) analysis.

2.2.3 Detection Conditions of UPLC-QE-MS/MS

Using a Waters UPLC BEH C18 column (1.7 μm*2.1*100 mm) and an Agilent ultra-high performance liquid chromatography 1290 UPLC system, LC-MS/MS analysis was carried out. The sample injection volume was set at 5 μL and the flow rate was set at 0.4 mL/min. 0.1% formic acid in water (A) and 0.1% formic acid in acetonitrile made up the mobile phase (B). The following was the multi-step linear elution gradient program: 0–3.5 min, 95–85% A; 3.5–6 min, 85–70% A; 6–6.5 min, 70–70% A; 6.5–12 min, 70–30% A; 12–12.5 min, 30–30% A; 12.5–18 min, 30–0% A; 18–25 min, 0-0 % A; 25–26 min, 0–95% A; 26–30 min, 95–95% A.

2.2.4 Data Processing and Chromatogram Acquisition

Raw mass spectrometry data were imported using XCMS software (Version 1.41.0, La Jolla, CA, USA). Retention time correction, peak identification, peak extraction, peak integration, peak alignment, etc., and the self-built secondary mass spectrometry database and the corresponding cleavage law matching method were used to identify the peaks containing MSMS data. Positive and negative ion modes were used to collect data on samples such as Astragalus-Safflower granules, rat drug-containing serum and rat blank serum, and the total ion chromatogram (TIC) was created.

2.3 Experimental Evidence

2.3.1 Experimental Animals

After one-week acclimatization, healthy male ApoE$^{-/-}$ mice weighing 18–20 g (Jiangsu Jizui Pharmachem Biotechnology Co., Nanjing, China; Animal license: SCXK [Jiangsu] 2018-0008) were kept in carefully regulated conditions, including a 12-h light/dark cycle, a temperature of 24 °C and 60% humidity with free access to food and drink. The Institutional Animal Care and Use Committee of Hainan Medical University approved all animal experimentation techniques (Number: HYLL-2021-140). The animal experiment followed Guidelines for Ethical Review of the Welfare of Laboratory Animals

Table 1. Primer sequences used for RT-qPCR analysis.

Gene Name	Forward	Reverse
β-actin	5′-CGTGACATTAAGGAGAAGCTG-3′	5′-CTAGAAGCATTTGCGGTGAC-3′
NLRP3	5′-ACAGCCACCTCACTTCCAG-3′	5′-CCAACCACAATCTCCGAATG-3′
Caspase-1	5′-AGAGGATTTCTTAAGGATGCA-3′	5′-TCACAAGACCAGGCATATTCTT-3′
GSDMD	5′-GGCCCTACTGCCTTCTG-3′	5′-AAAACACTCCGGTTCTGGT-3′
IL-1β	5′-AGTTGACGGACCCCAAA-3′	5′-TCTTGTTGATGTGCTGCTG-3′

in the People's Republic of China [GB/T 35892-2018].

2.3.2 Experimental Groups and Drug Treatment

Thirty mice were equally randomized into three groups: control group, model group, and ASHP (Huangqi-Honghua, HQ-HH) group. Animals in the control group were given normal chow, and those in model and ASHP groups were given high-fat chow for 12 weeks [26]. The high-fat feed was purchased from Changzhou Rat One Rat Two Biotechnology Co., Ltd., Changzhou, China; No. D12108C). Astragalus-Safflower was converted into a gavage dose for mice according to the dose commonly used in humans. A combination dose of Astragalus and Safflower was given at 4.5 g/kg/day and 1.5 g/kg/day. Mice were gavaged 0.2 mL each time, once a day for four weeks, and the experimental protocol was reviewed and approved by the ethics committee of Hainan Medical University. Animals in the control group received an equal amount of distilled water through intragastric administration. Under pentobarbital anesthesia, blood was taken through the abdominal aorta after the experiment. For biochemical analysis, serum was centrifuged at 4 °C and 3000 rpm for 15 min and then kept at –20 °C. For use in later investigations, the heart tissue was extracted during an autopsy and either promptly frozen in liquid nitrogen or preserved in 10% paraformaldehyde.

2.3.3 Heart Histopathology and Immunofluorescence

The heart tissue was dried, embedded in paraffin, fixed in 4% recent paraformaldehyde solution overnight, hematoxylin/eosin (H&E) stained, and sliced into (4 μm sections to observe the morphological structure of each specimen using an optical microscope (Eclipse Ci; Nikon, Tokyo, Japan) according to the manufacturer's instructions. For immunofluorescence staining, the frozen section of the mouse heart was fixed with 4% paraformaldehyde for 15 min, permeabilized with 0.1% Triton X-100 in phosphate-buffered saline (PBS), rinsed, and then incubated in 0.5% bovine serum albumin (BSA) in PBS for 30 min. The heart specimen was then incubated with a particular primary antibody at 4 °C overnight in an incubation buffer containing 1% BSA. The primary antibodies used were anti-NLRP3 (abs151406, Absin Bioscience Inc., Shanghai, China) , anti-Caspase-1 (abs155181, Absin Bioscience Inc., Shanghai, China), anti-GSDMD (#39754, Cell Signaling Technology, Danvers, MA, USA), anti-IL-1β (abs131179, Absin Bioscience). The heart slices were incubated with secondary antibodies for 1 h at room temperature after three washes with PBS and photographed with Nikon fluorescence microscope. Quantification analysis were performed by ImageJ software (Version 1.53, Bethesda, MD, USA).

2.3.4 Real-Time Quantitative Polymerase Chain Reaction (RT-qPCR)

Mouse heart tissue RNA was extracted using the Eastep super total RNA extraction kit (Promega, Shanghai, China) according to the manufacturer's instructions. A total of 2 μg RNA was reverse transcribed into cDNA (YEASEN Biotechnology, Shanghai, China). The qPCR system (Quantagene q225-0304, Kubo Tech Co, Zurich, Switzerland) was then used to amplify the target genes according to the Reverse Transcription Kit to develop the following cycling conditions: predenaturation at 95 °C for 5 min; denaturation at 95 °C 10 s, annealing to 60 °C for the 30 s, and 40 cycles. Relative mRNA expression was analyzed by the $2^{-\Delta\Delta Ct}$ method to analyze the data. Primers were designed on PubMed and synthesized by Beijing Prime Biotechnology Co. (Beijing, China). The primers used are listed in Table 1.

2.3.5 Western Blot Analysis

The mouse heart tissue was cut into small pieces, and the myocardial tissue was lysed by adding RIPA lysis solution to extract the total protein. The protein concentration was determined according to the instructions of the BCA Protein Assay Kit. An equal amount of protein (20 μg) was separated using sodium dodecyl sulfate-polyacrylamide gel electrophoresis (SDS-PAGE) before being transferred to a polyvinylidene fluoride (PVDF) membrane. After blocking with 5% milk, the membrane was cut according to molecular weight and then incubated overnight at 4 °C with rabbit anti-NLRP3 (1:1000, Absin Biotechnology, Shanghai, China), rabbit anti-Caspase-1 (1:1000, Absin Biotechnology,Shanghai, China), rabbit anti-GSDMD (1:1000, Cell Signaling Technology, Danvers, MA, USA), and rabbit anti-IL-1β (1:1000, Absin Biotechnology,Shanghai, China). The secondary antibody was incubated for 1 h at room temperature. The ECL kit was utilized to find the signal (310208, ZETA, Menlo Park, CA, USA). Western blotting results were analyzed using ImageJ software and displayed using GraphPad Prism (Version 8.0, San Diego, CA, USA).

2.4 Data Analysis

Data are presented as the mean ± standard deviation (SD) and were analyzed by GraphPad Prism 8.0. Statistical comparisons of multiple groups were performed using one-way ANOVA. The results were considered statistically significant when the *p* value was less than 0.05.

3. Results

3.1 Screening for Active Compounds and Targets of ASHP

The chemical composition of ASHP was searched through the TCMSP database. The major components of ASHP were screened by OB ≥30% and DL ≥0.18, and finally 20 major components of Astragalus and 34 major components of Safflower were obtained (**Supplementary Table 1**). After removing the duplicates, there were 188 targets corresponding to Astragalus and 216 targets corresponding to Safflower.

3.2 CHD-Related Targets and Common Targets between Astragalus-Safflower and CHD

Altogether 1576 CHD-related targets were discovered by searching the databases of DisGeNET. Some of the CHD-related targets and the predictive targets of ASHP are overlapping. After removing any duplicate targets, 90 potential ASHP targets for CHD were identified (Fig. 2), which are detailed in **Supplementary Table 2**.

3.3 Construction of the PPI Network and Scanning of Hub Genes

The PPI network of the herb compound-disease target interactions for the 90 over-lapping targets was constructed using the STRING database. From the analysis, we chose a score greater than 0.7. The PPI network had 90 nodes and 1379 edges, with a mean node degree of 30.6 and a local clustering coefficient on the order of 0.699 (as shown in Fig. 3A). After analysis using the cytohub plugin in Cytoscape software, the top 10 key genes were ranked according to the degree of display integrity. The 10 hub genes were *IL6, AKT1, IL1B, TP53, VEGFA, PTGS2, MMP9, CCL2, CXCL8* and *EGF* (Fig. 3B). Topologically, the most important node in the network has betweenness centrality, the highest degree, and closeness centrality. The quantity of edges that are connected to a node determines its "degree". The quantity of shortest paths passing through a certain node is known as "betweenness" . The quantity of average diastance from a certain node is known as "closeness". The features of hub genes are displayed in Table 2 [27].

3.4 Construction of the Compound-Target-Disease (C-T-D) Network

The disease, compounds and overlapping genes were imported into Cytoscape software to map a "compound-target-disease" network graph, which showed 121 nodes and 508 edges, containing 1 disease name, 30 compounds, and 90 targets (Fig. 4).

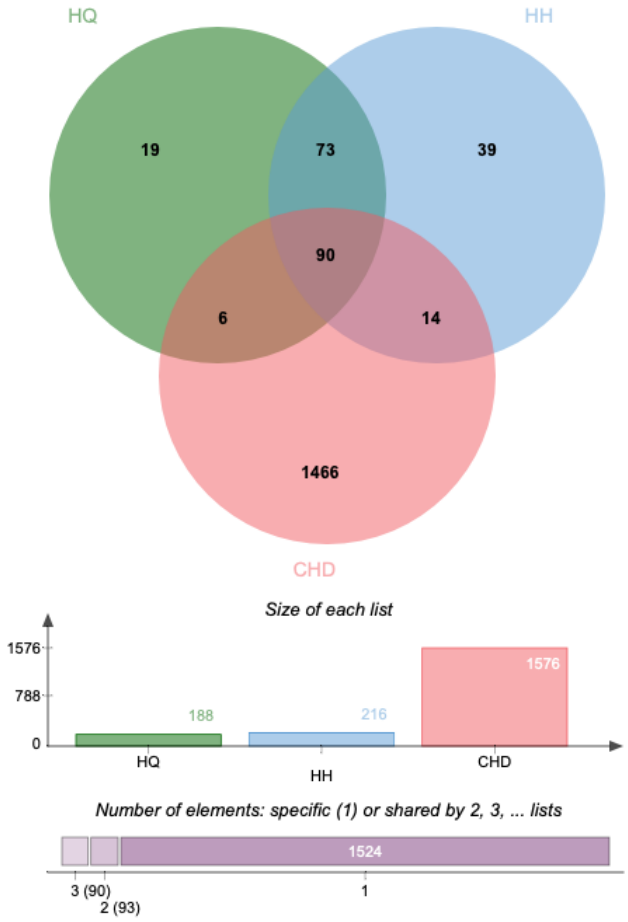

Fig. 2. Venn diagram of overlapping genes associated with CHD in ASHP.

Table 2. The characteristics of top 10 hub genes.

Gene	Degree	Betweenness	Closeness
IL6	71	409.44446	0.8240741
AKT1	71	522.7065	0.8317757
IL1B	65	220.52296	0.78070176
TP53	64	233.48093	0.78070176
VEGFA	64	181.15057	0.773913
PTGS2	60	245.07791	0.7542373
MMP9	55	85.41447	0.7177419
CCL2	55	96.76832	0.7177419
CXCL8	55	94.17428	0.7177419
EGF	55	156.39207	0.7177419

3.5 Results of GO Enrichment Analysis

The overlapping genes were analyzed by the Metascape database for GO enrichment analysis, including the biological process (BP), cell composition (CC), and molecular function (MF) (Figs. 5 and 6). The top 20 BP are presented, mainly including the following: positive regulation of cell motility, response to an inorganic substance, and response to the hormone (Table 3). The top 20 MF are presented, mainly including RNA polymerase II-specific

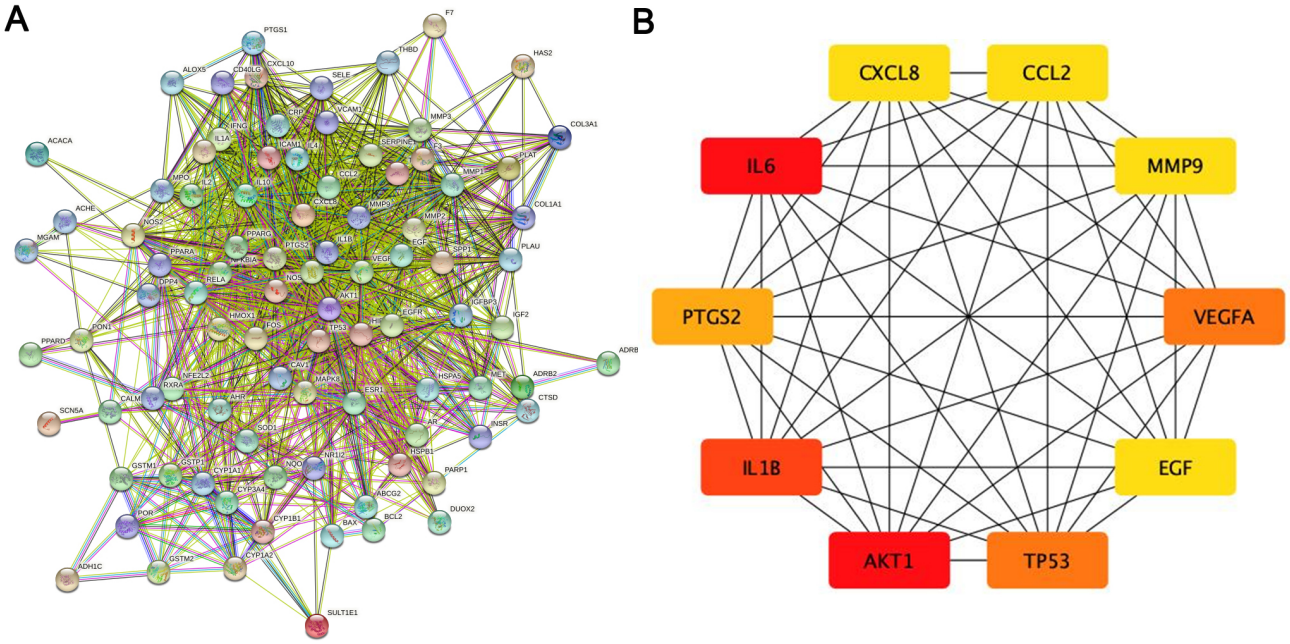

Fig. 3. The main targets and network of ASHP in the treatment of CHD. (A) Protein-protein interaction network of ASHP in the treatment of CHD. (B) The top 10 hub gene of ASHP in the treatment of CHD.

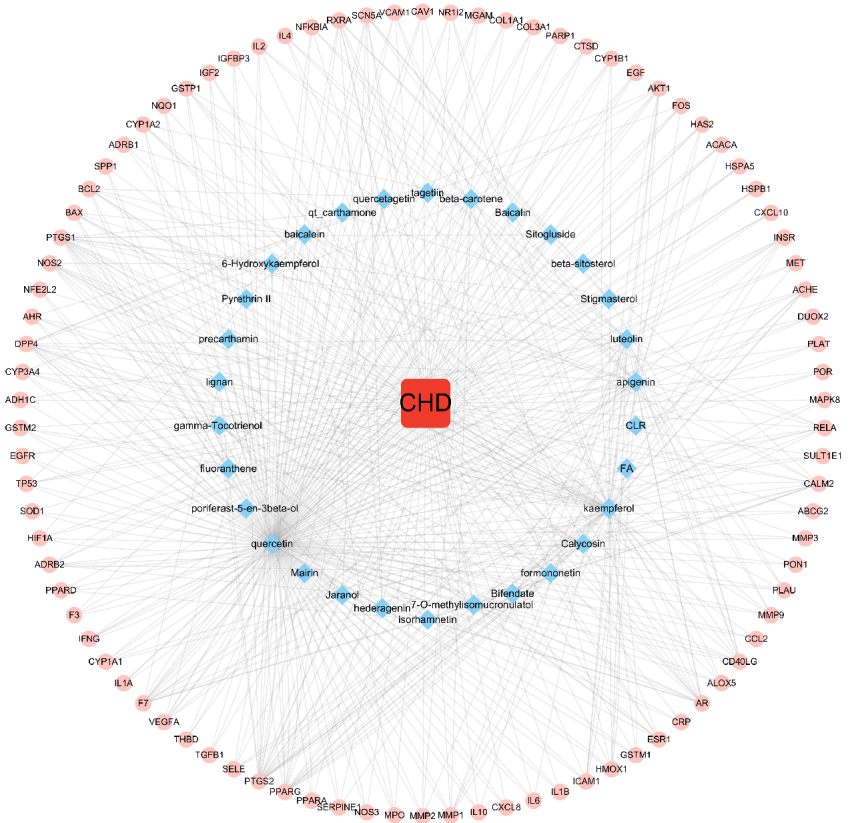

Fig. 4. C-T-D Network Construction of ASHP in the treatment of CHD.

DNA-binding transcription factor binding and cytokine activity (Table 4); The top 20 CC are presented, mainly including the membrane raft, extracellular matrix, vesicle lumen and heme binding (Table 5).

3.6 Results of KEGG Enrichment Analysis

Enrichment analysis of the overlapping genes for the KEGG signaling pathway was performed through the Metascape database. The top 20 ranked KEGG path-

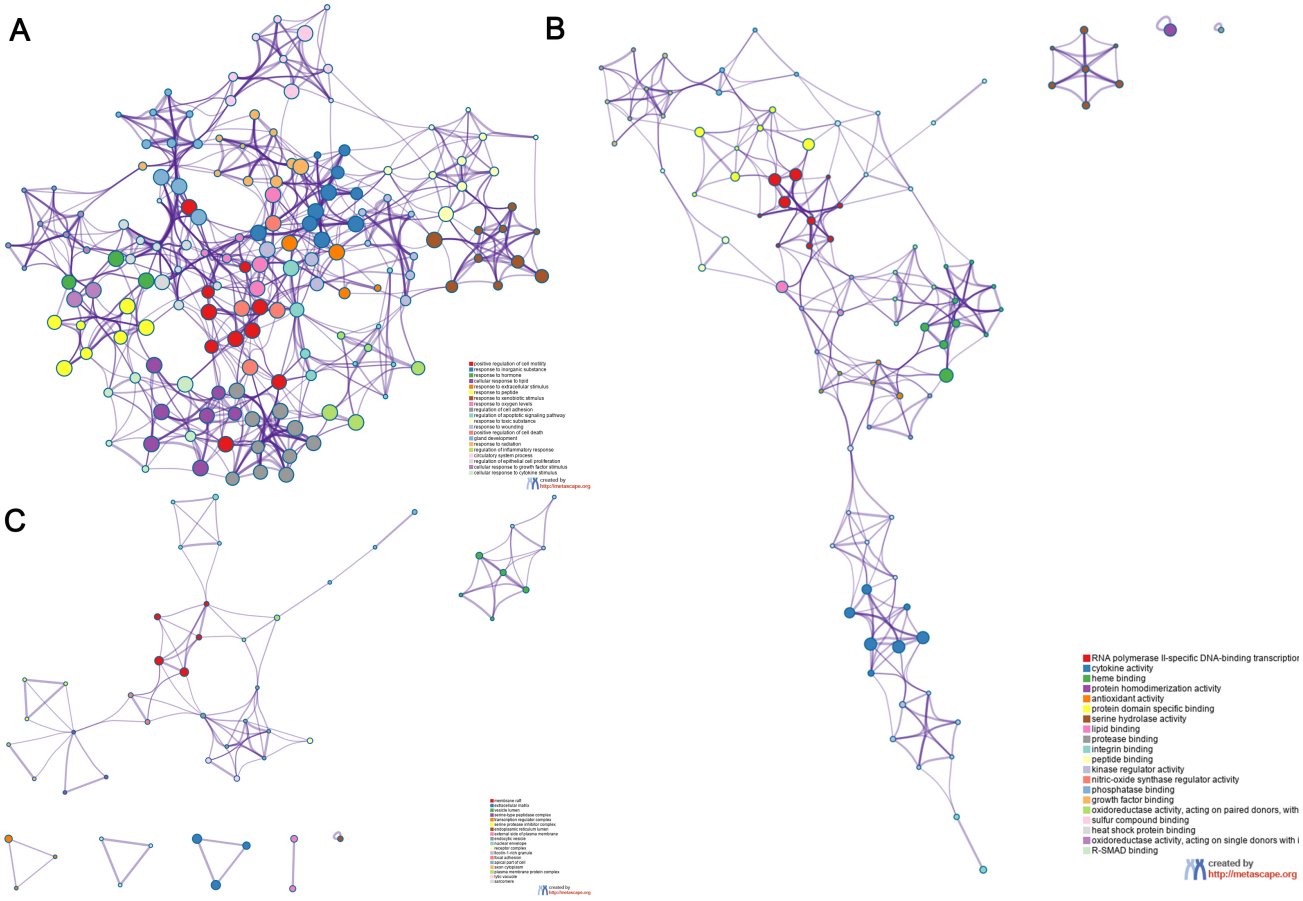

Fig. 5. Go functional enrichment analysis of the top 20 results from enrichment analysis of overlapping genes. GO analysis of terms for (A) BP, (B) MF, and (C) CC. Each cluster ID is indicated with a specific color. Each term is represented by a circular node, whose size corresponds to the term's number of input genes, and whose color indicates membership in the same cluster.

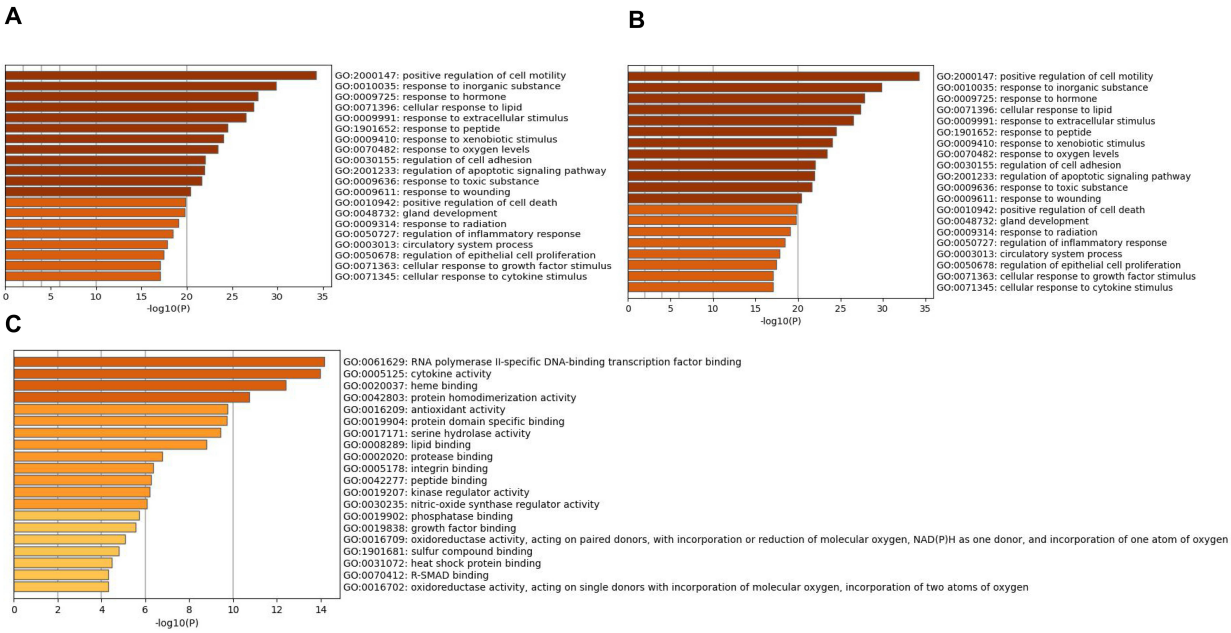

Fig. 6. Go enrichment analysis of overlapping genes Bar graph showing the top 20 results of targets for Astragalus-Safflower drug pairs against CHD. (A) BP terms (B) MF terms and (C) CC terms. The x-axis values correspond to $-\log_{10}(p)$ values. The biological processes are more significant the higher the value.

Table 3. GO analysis of overlapping genes (BP terms).

GO	Description	Count	%	$Log_{10}(p)$	$Log_{10}(q)$
GO:2000147	positive regulation of cell motility	34	37.78	–34.26	–30.18
GO:0010035	response to inorganic substance	30	33.33	–29.84	–26.35
GO:0009725	response to hormone	32	35.56	–27.80	–24.39
GO:0071396	cellular response to lipid	28	31.11	–27.35	–24.00
GO:0009991	response to extracellular stimulus	27	30.00	–26.47	–23.28
GO:1901652	response to peptide	25	27.78	–24.50	–21.46
GO:0009410	response to xenobiotic stimulus	24	26.67	–24.05	–21.04
GO:0070482	response to oxygen levels	22	24.44	–23.44	–20.48
GO:0030155	regulation of cell adhesion	28	31.11	–22.04	–19.17
GO:2001233	regulation of apoptotic signaling pathway	22	24.44	–21.93	–19.09
GO:0009636	response to toxic substance	19	21.11	–21.66	–18.85
GO:0009611	response to wounding	22	24.44	–20.41	–17.67
GO:0010942	positive regulation of cell death	24	26.67	–19.85	–17.16
GO:0048732	gland development	21	23.33	–19.75	–17.08
GO:0009314	response to radiation	21	23.33	–19.05	–16.43
GO:0050727	regulation of inflammatory response	20	22.22	–18.42	–15.84
GO:0003013	circulatory system process	21	23.33	–17.86	–15.33
GO:0050678	regulation of epithelial cell proliferation	19	21.11	–17.45	–14.96
GO:0071363	cellular response to growth factor stimulus	20	22.22	–17.10	–14.62
GO:0071345	cellular response to cytokine stimulus	23	25.56	–17.06	–14.60

Table 4. GO analysis of overlapping genes (MF terms).

GO	Description	Count	%	$Log_{10}(p)$	$Log_{10}(q)$
GO:0061629	RNA polymerase II-specific DNA-binding transcription factor binding	16	17.78	–14.17	–10.58
GO:0005125	cytokine activity	14	15.56	–13.97	–10.58
GO:0020037	heme binding	11	12.22	–12.40	–9.56
GO:0042803	protein homodimerization activity	17	18.89	–10.73	–8.22
GO:0016209	antioxidant activity	8	8.89	–9.74	–7.31
GO:0019904	protein domain specific binding	16	17.78	–9.71	–7.30
GO:0017171	serine hydrolase activity	10	11.11	–9.42	–7.03
GO:0008289	lipid binding	16	17.78	–8.78	–6.42
GO:0002020	protease binding	7	7.78	–6.75	–4.57
GO:0005178	integrin binding	7	7.78	–6.35	–4.20
GO:0042277	peptide binding	9	10.00	–6.27	–4.15
GO:0019207	kinase regulator activity	8	8.89	–6.20	–4.10
GO:0030235	nitric-oxide synthase regulator activity	3	3.33	–6.05	–4.01
GO:0019902	phosphatase binding	7	7.78	–5.73	–3.71
GO:0019838	growth factor binding	6	6.67	–5.54	–3.53
GO:0016709	oxidoreductase activity, acting on paired donors, with incorporation or reduction of molecular oxygen, NAD(P)H as one donor, and incorporation of one atom of oxygen	4	4.44	–5.08	–3.13
GO:1901681	sulfur compound binding	7	7.78	–4.79	–2.89
GO:0031072	heat shock protein binding	5	5.56	–4.46	–2.60
GO:0016702	oxidoreductase activity, acting on single donors with incorporation of molecular oxygen, incorporation of two atoms of oxygen	3	3.33	–4.31	–2.47
GO:0070412	R-SMAD binding	3	3.33	–4.31	–2.47

ways are presented, mainly including fluid shear stress, atherosclerosis, cancer-related pathways, activation of chemical carcinogenesis-receptors, interleukin (IL)-17 signaling pathway, malaria, and relaxin signaling pathway (Fig. 7A,B; Table 6). We selected 10 pathways with high relevance to CHD for KEGG signaling pathway using Sankey bubble plots. The left side of this figure is a Sankey diagram, representing the genes contained in each pathway, and the right side is a regular bubble diagram, with the bubble size indicating the number of genes belonging

Table 5. GO analysis of overlapping genes (CC terms).

GO	Description	Count	%	$Log_{10}(p)$	$Log_{10}(q)$
GO:0045121	membrane raft	13	14.44	–10.78	–7.77
GO:0031012	extracellular matrix	14	15.56	–8.81	–6.16
GO:0031983	vesicle lumen	10	11.11	–7.29	–4.90
GO:1905286	serine-type peptidase complex	4	4.44	–7.29	–4.90
GO:0005667	transcription regulator complex	11	12.22	–6.57	–4.28
GO:0097180	serine protease inhibitor complex	3	3.33	–6.29	–4.07
GO:0005788	endoplasmic reticulum lumen	8	8.89	–5.37	–3.31
GO:0009897	external side of plasma membrane	9	10.00	–5.01	–3.00
GO:0030139	endocytic vesicle	7	7.78	–4.12	–2.18
GO:0005635	nuclear envelope	8	8.89	–3.99	–2.06
GO:0043235	receptor complex	8	8.89	–3.65	–1.74
GO:0101002	ficolin-1-rich granule	5	5.56	–3.63	–1.74
GO:0005925	focal adhesion	7	7.78	–3.57	–1.70
GO:0045177	apical part of cell	7	7.78	–3.53	–1.70
GO:1904115	axon cytoplasm	3	3.33	–3.07	–1.30
GO:0098797	plasma membrane protein complex	8	8.89	–2.89	–1.14
GO:0000323	lytic vacuole	8	8.89	–2.78	–1.07
GO:0030017	sarcomere	4	4.44	–2.44	–0.78
GO:0045121	membrane raft	13	14.44	–10.78	–7.77
GO:0031012	extracellular matrix	14	15.56	–8.81	–6.16

Table 6. KEGG analysis of overlapping genes.

GO	Description	Count	%	$Log_{10}(p)$	$Log_{10}(q)$
hsa05418	Fluid shear stress and atherosclerosis	27	30	–41.53	–38.99
hsa05200	Pathways in cancer	37	41.11	–40.45	–38.21
hsa05207	Chemical carcinogenesis- receptor activation	20	22.22	–23.95	–22.11
hsa04657	IL-17 signaling pathway	15	16.67	–21.53	–19.84
hsa05144	Malaria	12	13.33	–19.60	–18.06
hsa04926	Relaxin signaling pathway	15	16.67	–19.36	–17.86
hsa04066	HIF-1 signaling pathway	14	15.56	–18.71	–17.25
hsa05215	Prostate cancer	13	14.44	–17.65	–16.22
hsa04932	Non-alcoholic fatty liver disease	14	15.56	–16.50	–15.14
hsa05205	Proteoglycans in cancer	14	15.56	–14.79	–13.59
hsa05225	Hepatocellular carcinoma	13	14.44	–14.46	–13.28
hsa04064	NF-kappa B signaling pathway	11	12.22	–13.81	–12.7
hsa01522	Endocrine resistance	10	11.11	–12.43	–11.46
hsa05219	Bladder cancer	8	8.89	–12.40	–11.44
hsa04672	Intestinal immune network for IgA production	6	6.67	–8.13	–7.44
hsa04923	Regulation of lipolysis in adipocytes	6	6.67	–7.77	–7.09
hsa04371	Apelin signaling pathway	7	7.78	–6.69	–6.10
hsa04610	Complement and coagulation cascades	6	6.67	–6.67	–6.08
hsa04913	Ovarian steroidogenesis	5	5.56	–6.35	–5.79
hsa04217	Necroptosis	7	7.78	–6.29	–5.74

to the pathway and the bubble color indicating the *p*-value (Fig. 7C). Using the KEGG mapping color, we selected the Nod-like receptor signaling pathway for display (Fig. 8). The NLRP3-mediated proptosis pathway was seen in this pathway, which was confirmed by subsequent molecular docking and experimental verification.

3.7 Serum Drug Chemistry Analysis Results

The data were collected in positive and negative ion mode for Astragalus-Safflower granule, Astragalus-Safflower drug-containing serum and blank serum. The total ion flow chromatograms (TIC) are shown in **Supplementary Figs. 1** and **2**. A total of 489 positive ion serum drug compounds and 379 negative ion serum drug compounds were identified, and after comparison with the

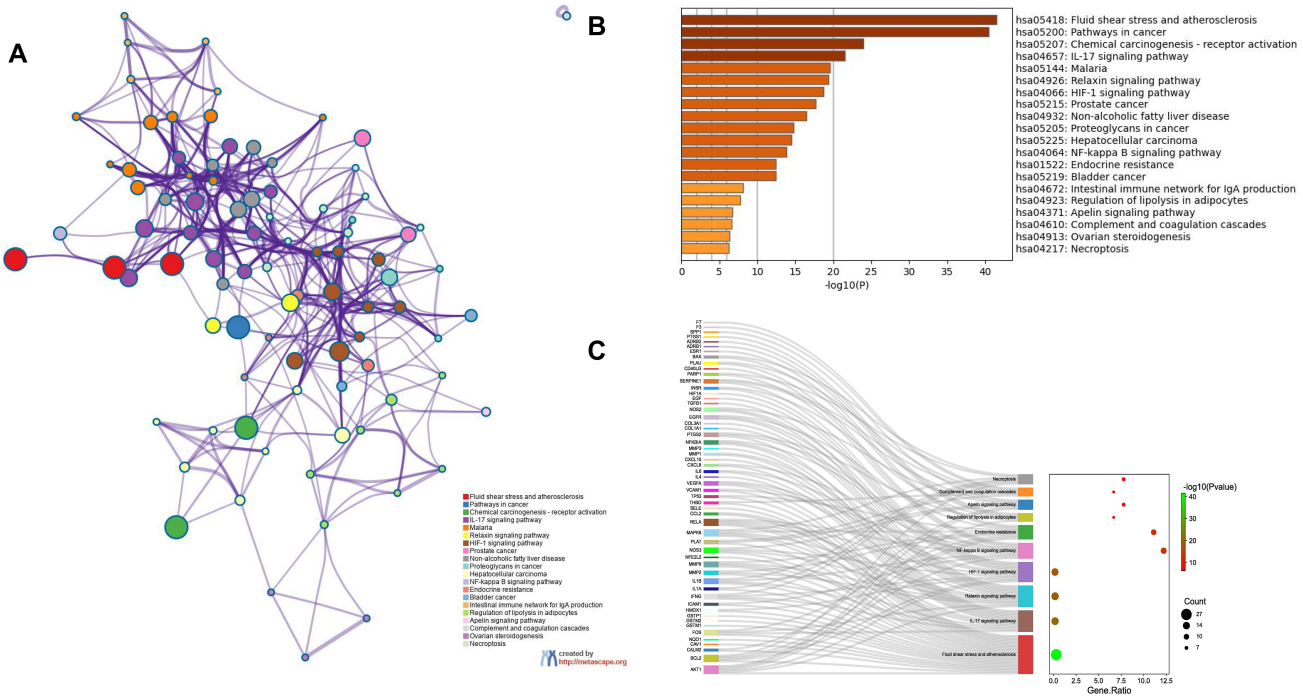

Fig. 7. Functional enrichment analysis of overlapping genes. (A) The network of enriched terms of overlapping genes; colors represent the same cluster ID. (B) Bar graph of KEGG analysis of overlapping genes. *p* value is shown in color. (C) Sankey plots show 10 pathways involved in KEGG enrichment pathways associated with CHD. The Sankey diagram on the left represents the genes contained in each pathway, and the regular bubble diagram on the right, with bubble size indicating the number of genes belonging to the pathway and bubble color indicating the *p*-value.

database, 2 negative ion mode blood compounds were finally obtained, which were calycosin and isorhamnetin (marked with 1.2 in **Supplementary Fig. 2**, **Supplementary Table 3**). Two serum compounds were compared with the Astragalus-Safflower that we retrieved in the TCMSP database, the results show that calycosin and isorhamnetin were in the core compound table obtained from this database.

3.8 Molecular Docking of Core Active Compounds and Proteins

The core targets of the NLRP3-mediated proptosis pathway, NLRP3 (PDB: 7ALV) [28], Caspase-1 (PDB: 5FNA) [29], and Astragalus-Safflower were selected for molecular docking analysis of the screened active ingredient quercetin, kaempferol and apigenin. Meanwhile, Molecular docking of the two entry compounds calycosin and isorhamnetin identified from Astragalus-Safflower rat serum with NLRP3 and Caspase-1 proteins. The docking results are shown in Table 7 and Fig. 9. It was found that the molecular docking binding energy was $\leq$–5.0 kJ/mol, and hydrogen bonds could be formed, indicating that the ligand and receptor could bind well and had stable structure after binding.

Table 7. The active compounds of ASHP docking with the potential targets.

Compounds	Targets	PDB ID	Score, kJ/mol
quercetin	NLRP3	7ALV	–6.2744
kaempferol	NLRP3	7ALV	–6.1576
apigenin	NLRP3	7ALV	–5.8945
calycosin	NLRP3	7ALV	–6.1122
isorhamnetin	NLRP3	7ALV	–6.1980
quercetin	Caspase-1	5FNA	–6.0698
kaempferol	Caspase-1	5FNA	–6.1021
apigenin	Caspase-1	5FNA	–6.0009
calycosin	Caspase-1	5FNA	–6.3561
isorhamnetin	Caspase-1	5FNA	–6.4310

3.9 Construction of the "Core Active Compound-Target" Network

According to the aforementioned study, the core active compounds of ASHP were quercetin, kaempferol, apigenin, calycosin and isorhamnetin. The core active compounds and targets were imported into Cytoscape software to map a "core active compound-target-disease" network graph, which showed 198 nodes and 328 edges, containing 1herb pair, 5 core active compounds, and 192 targets (Fig. 10).

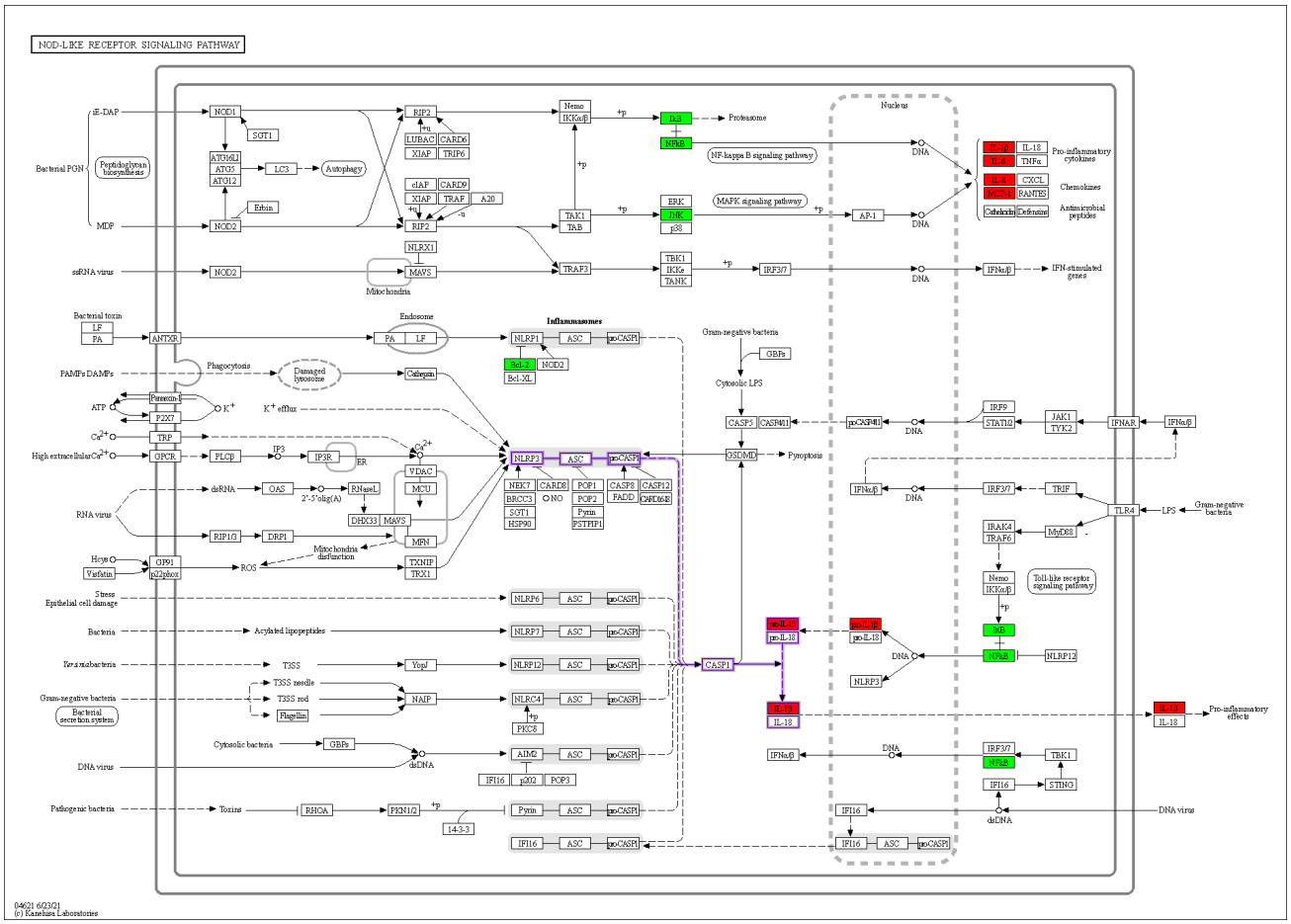

Fig. 8. Nod-like receptor signaling pathway. Overlapping genes in green, hub genes in red, and NLRP3 inflammasome-mediated pyroptosis pathway are shown in purple.

3.10 Comparison of Myocardial Pathomorphology in Mice

In the normal group, the myocardium was evenly stained; the cell shape was intact and closely arranged; the nucleus was centered with no break or defect; and no inflammatory cell infiltration was seen. In the CHD model group, myocardial cells were changed in shape and disordered in arrangement with widened myocardial gaps; the nuclei were fixed, some of which were edematous and deformed; and a small amount of inflammatory cell infiltration was seen. In ASHP group (HQ-HH), the cell shape and arrangement of the myocardial tissue improved significantly; the myocardial gap was narrowed; and the inflammatory cell infiltration and nuclear consolidation were significantly reduced (Fig. 11).

3.11 ASHP Inhibits the Expression of Key Pyroptosis Proteins in Mice with CHD Model

To confirm the findings from the KEGG pathway, we selected the four highly linked targets (NLRP3, Caspase-1, GSDMD, IL-1β) for experimental verification based on the network pharmacology analysis. Immunofluorescence double-staining detected the protein expression of NLRP3 and Caspase-1 in the mouse heart tissue, and an increasing trend in the model group compared with the control group ($p < 0.01$), while the protein expression level of NLRP3 and Caspase-1 was decreased after ASHP intervention ($p < 0.05$) (Fig. 12A). Similarly, GSDMD and IL-1β immunofluorescence double staining of myocardial tissue of mice was also observed in CHD model mice, and the expression of GSDMD and IL-1β decreased with the intervention of Astragalus-Safflower drugs (Fig. 12B). RT-qPCR analysis was used to measure the mRNA expression of NLRP3 and Caspase-1 mRNA expression levels in the mouse heart tissue. As shown in Fig. 13, the mRNA expression levels of NLRP3, Caspase-1, GSDMD, and IL-1β in the model group were significantly higher than those in the control group ($p < 0.01$). In contrast to the model group, HQ-HH group displayed a drop in NLRP3 and caspase-1 transcriptional levels ($p < 0.01$). Next, we examined the protein expression of NLRP3, Caspase-1, GSDMD, IL-1β by Western blotting. As shown in Fig. 14, the expression of NLRP3, Caspase-1, GSDMD, and IL-1β were markedly increased in the CHD model, whereas treating with Astragalus-Safflower significantly inhibited expression.

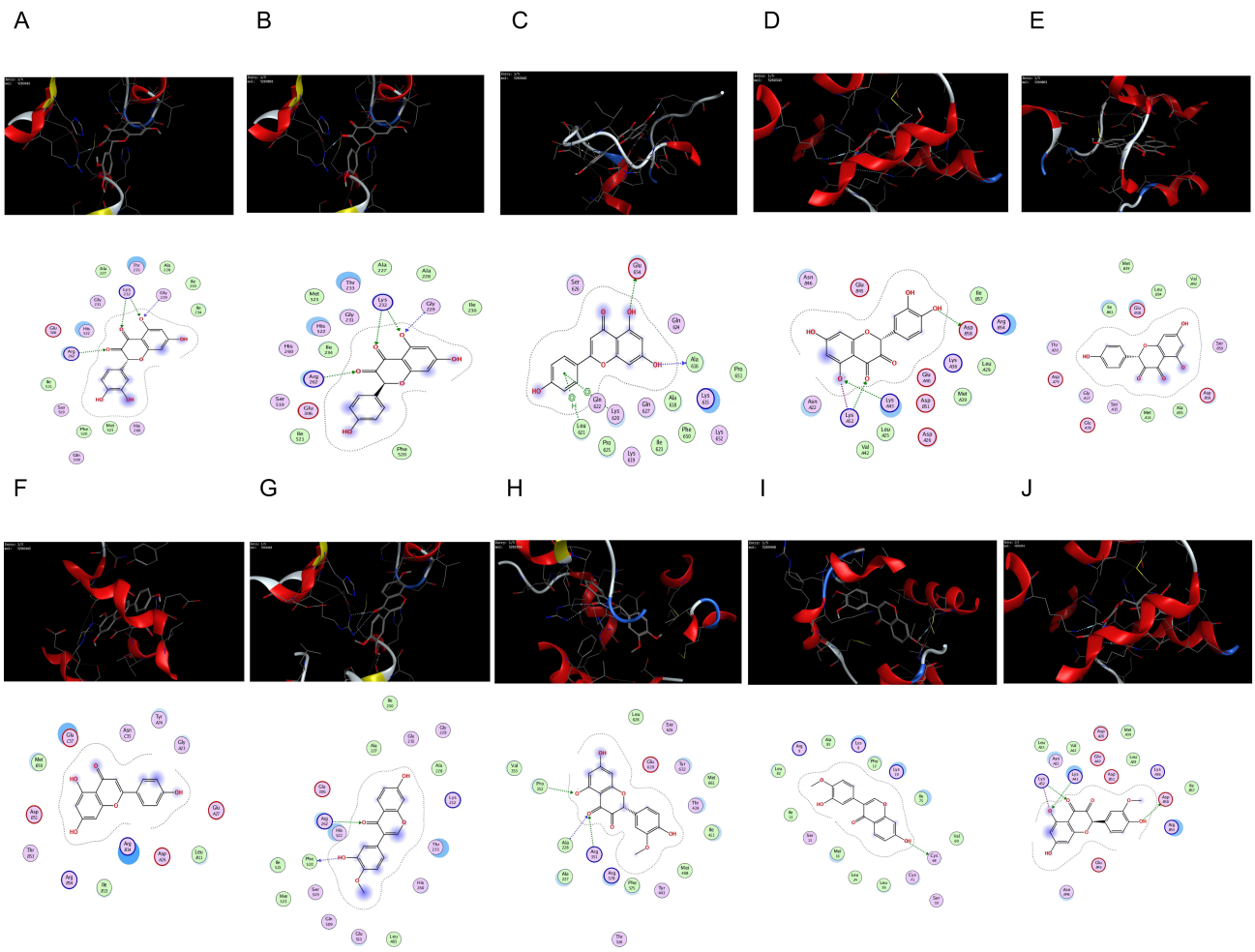

Fig. 9. The network of molecular docking results. (A) quercetin interacting with NLRP3. (B) kaempferol interacting with NLRP3. (C) apigenin interacting with NLRP3. (D) quercetin interacting with Caspase-1. (E) kaempferol interacting with Caspase-1. (F) apigenin interacting with Caspase-1. (G) calycosin interacting with NLRP3. (H) isorhamnetin interacting with NLRP3. (I) calycosin interacting with Caspase-1. (J) isorhamnetin interacting with Caspase-1.

4. Discussion

CVD is a common disease in people over 50 years of age. About 330 million people are affected by various cardiovascular diseases in China, of which CHD is one of the main causes of morbidity [2]. CHD is a multifactorial and complex disease. Secondary prevention of CHD is still the basic principle of western medicine for the treatment of coronary artery disease (CAD). Antiplatelet and statin drugs are the cornerstone of CAD treatment, but their adverse effects include gastrointestinal adverse effects, bleeding events, antiplatelet drug resistance, and liver function impairment and rhabdomyolysis. Most of these drugs are single-targeting, and most of these studies have focused on the single pathway related to the disease.

TCM have the advantages of multi-targets and multi-pathways. According to the TCM theory, the most common type of CHD is qi stagnation and blood deficiency, and Astragalus and Safflower are the representative drugs of relieving qi stagnation and blood deficiency, respectively. In addition, Astragalus is used to tonify qi and promote the operation of qi, while Safflower is representative of invigorating blood circulation and removing blood stasis. When these two herbal drugs are combined, one plays an eliminating role and the other plays a tonifying role; one treats deficiency and the other treats actual symptoms to achieve the ultimate therapeutic effect of tonifying qi and removing blood stasis. The studies have shown that the primary ingredients of Huangqi-Honghua combination and their antioxidant function alleviate cerebral infarction with qi deficit and blood stasis syndrome. The primary active components of Astragalus-Safflower are AS-IV and HSYA. When these two substances were combined, they significantly reduced the infarct volume in rats 24 hours after reperfusion by increasing the expression of nuclear factor erythroid-associated factor 2 (Nrf2) and the antioxidant activity, which reduced levels of malondialdehyde (MDA) and reactive oxygen species (ROS) [8]. However, the application and mechanism of action of ASHP in CHD have

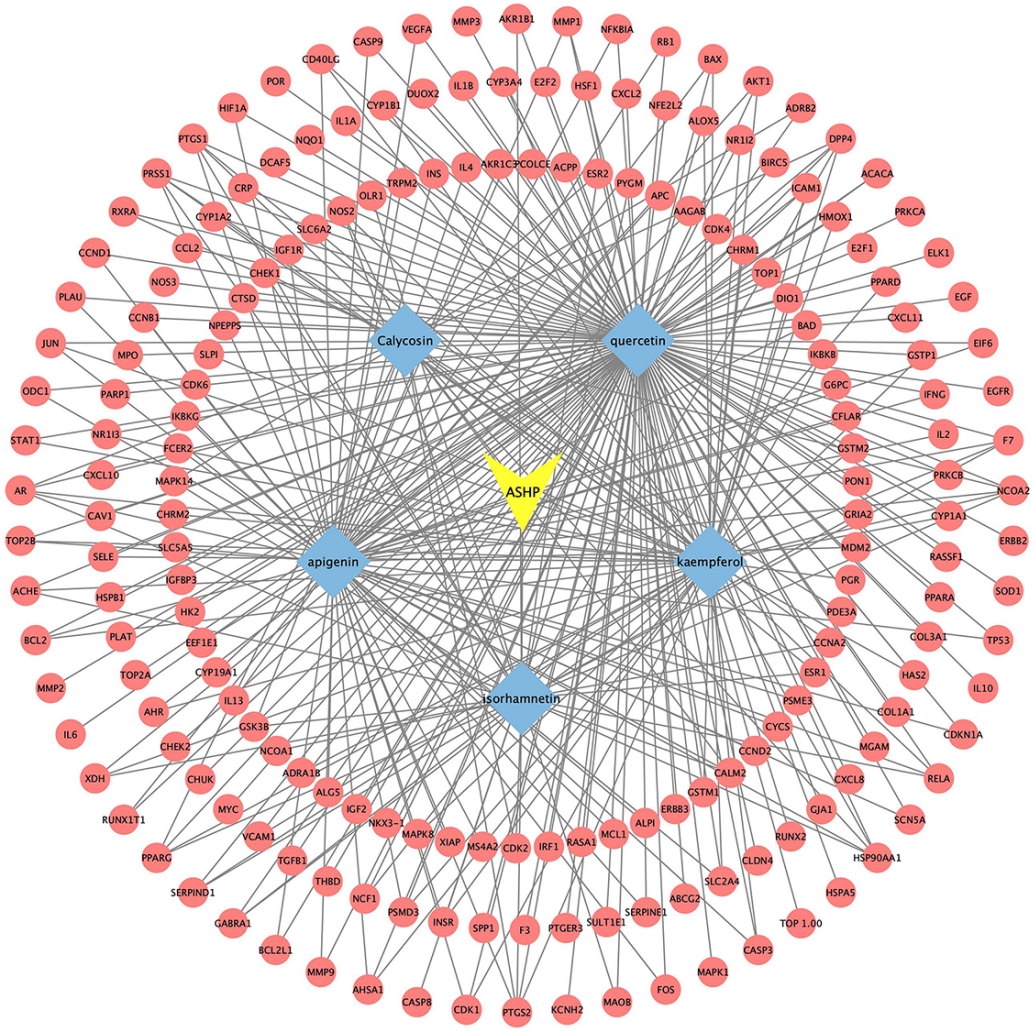

Fig. 10. Core Active Compound-Target Network Construction of ASHP.

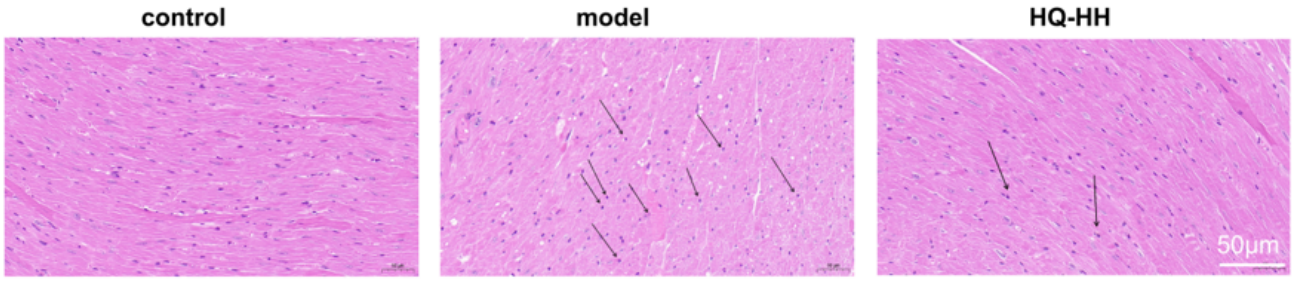

Fig. 11. HE staining of myocardial pathology in groups of mice (×20).

not been reported.

In this study, we used network pharmacology and molecular docking to analyze ASHP and explore the pharmacodynamic mechanism of the herb pair in the treatment of CHD. The mechanism of illness and therapeutic activity is explained by network pharmacology from the broad perspective of biological networks. It is a new field created to see how medications interact with illness based on system pharmacology and bioinformatics. In this study, we finally obtained 20 major compounds of Astragalus and 188 corresponding targets, and 34 major components of Safflower and 216 corresponding targets through screening. We construct a sub-network of the main core compounds and targets, the results showed that a single chemical component could have multiple corresponding targets, and at the same time, different chemical components could intersect on the same target, which reflects the characteristics of ASHP with multiple targets and rich effects [30–32]. The main components of ASHP are quercetin (PubChem CID: 5280343), kaempferol (PubChem CID: 5280863) and apigenin (Pub-

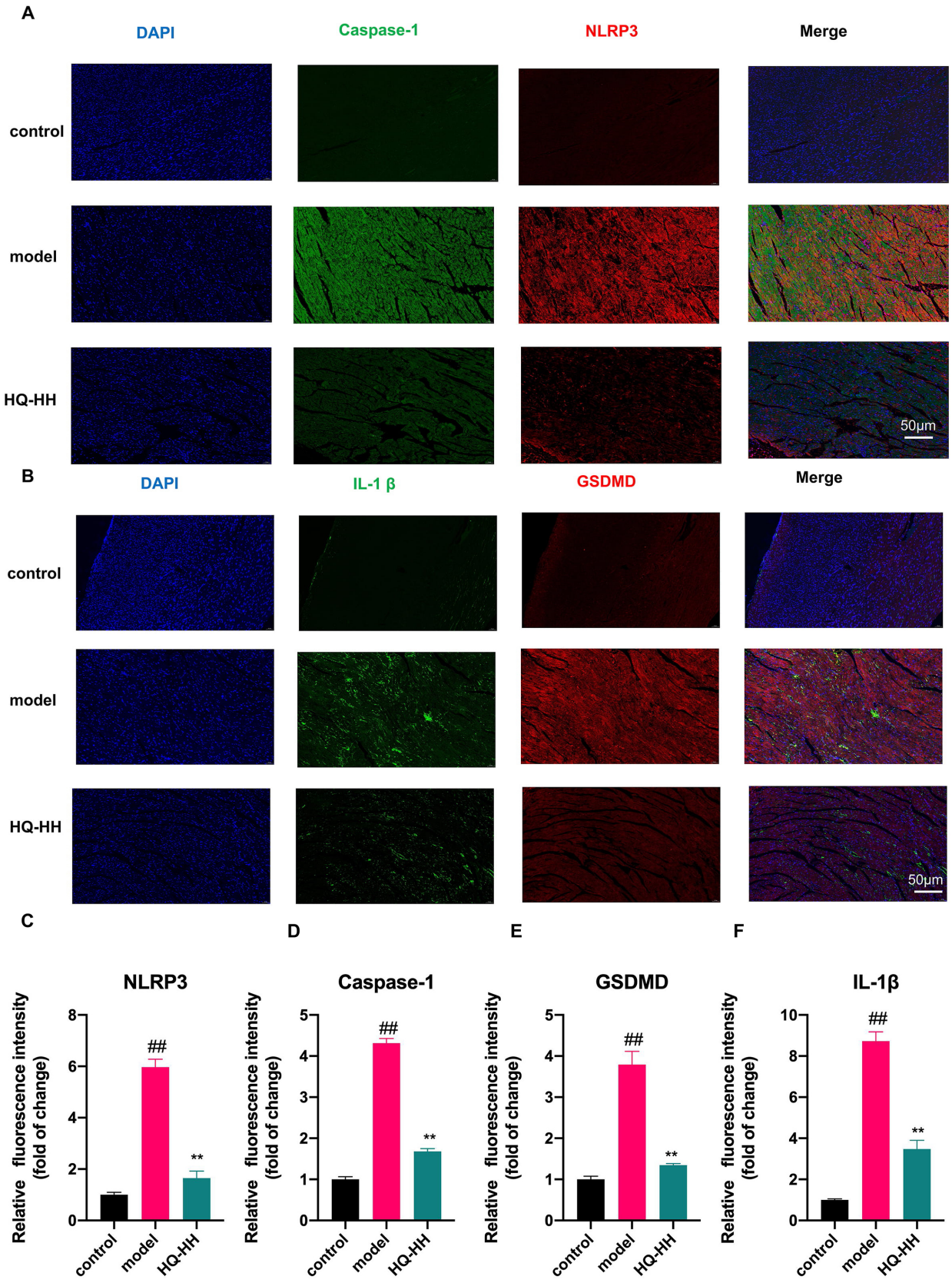

Fig. 12. Immunofluorescence double-staining of myocardial pathology in groups of mice (×20). (A) Expression of NLRP3 and Caspse-1 in mouse myocardial tissue by gimmunofluorescence, (B) Expression of GSDMD and IL-1β in mouse myocardial tissue by gimmunofluorescence, (C)–(F) Statistical values of immunofluorescence intensity of NLRP3, Caspse-1, GSDMD and IL-1β protein in each group. The data are shown as the mean $\pm$ SD. $^{\#\#}$ $p < 0.01$ versus the control group; ** $p < 0.01$ versus the model group.

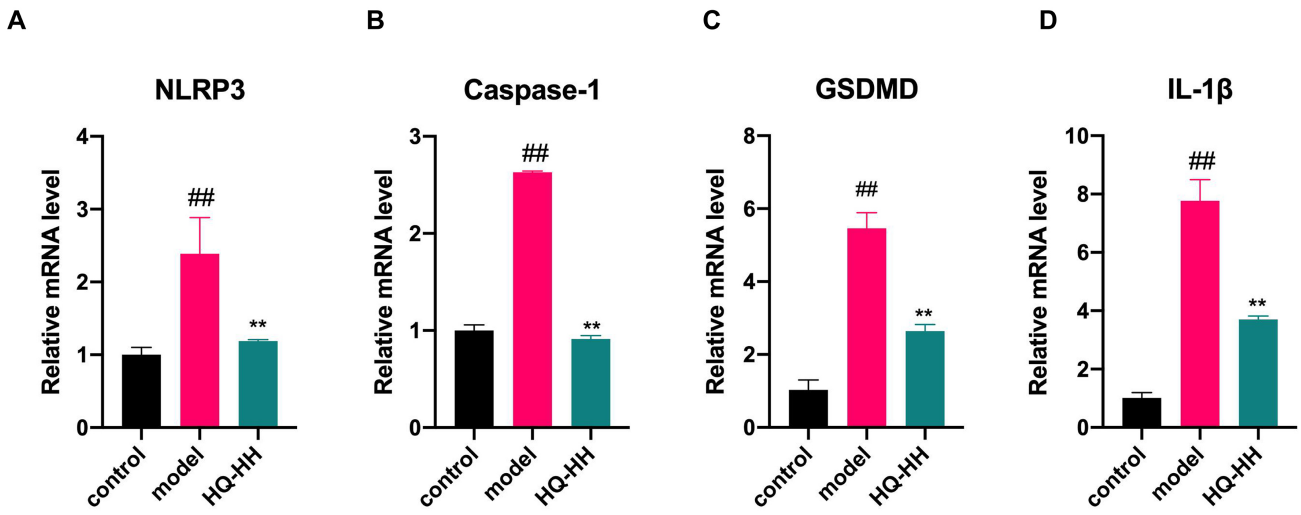

Fig. 13. Effects of Astragalus-Safflower drug pair on the mRNA expression of NLRP3, Caspase-1, GSDMD and IL-1β in different groups. NLRP3 (A) , Caspase-1 (B) , GSDMD (C) and IL-1β (D) mRNAs were measured by RT-qPCR, and the expression levels were normalized to β-actin. All data are presented as the mean $\pm$ SD. $^{\#\#}$ $p < 0.01$ versus the control group; ** $p < 0.01$ versus the the model group.

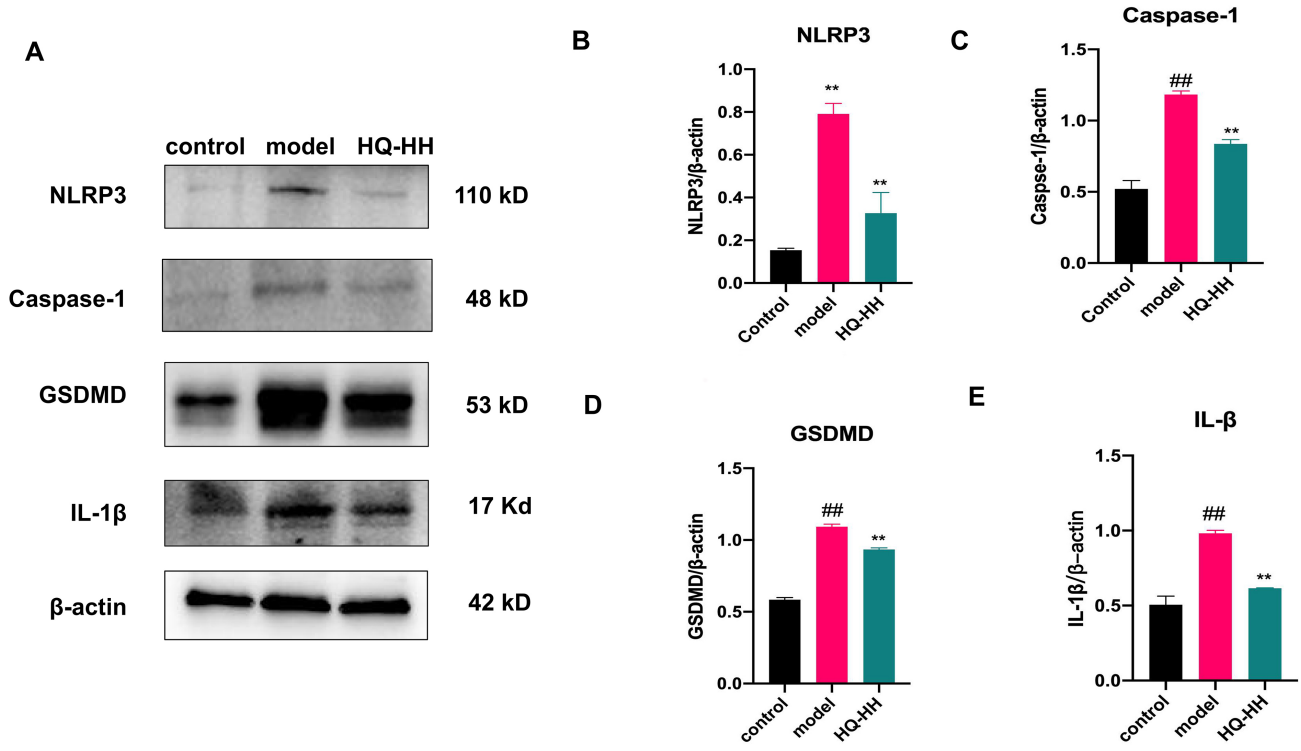

Fig. 14. Expression of NLRP3, Caspase-1, GSDMD and IL-1β protein in myocardial tissue of mice in each group. Protein expression of NLRP3, Caspase-1, GSDMD and IL-1β was analyzed by Western blotting (A). (B)–(E) The greyscale values of the bands were quantified by Image J software. The data are shown as the mean $\pm$ SD. $^{\#\#}$ $p < 0.01$ versus the control group; ** $p < 0.01$ versus the model group.

Chem CID: 5280443) as shown by network pharmacology. The study showed that by controlling the SIRT3/PARP-1 pathway, quercetin preserved the mitochondrial activity and helped prevent heart hypertrophy [33]. Quercetin has been shown to decrease the effects of oxidative stress, vascular rarefaction, cardiomyocyte hypertrophy, cardiac fibrosis and cardiac fat storage brought on by High-fat diet (HFD) [34]. Studies have shown that quercetin can promote the conversion of cholesterol to bile acids and cholesterol efflux, reduce aortic plaque area, oxidized low density

lipoprotein (ox-LDL) accumulation and foam cell formation, thus achieving the anti-atherosclerotic effect [35,36]. According to the research, kaempferol medication prevents ventricular hypertrophy, and this cardio-protection may be partly attributed to kaempferol's suppression of the ASK1/MAPK signaling pathway and its control of oxidative stress [37]. A large number of studies have shown that apigenin can play an anti-atherosclerotic effect by reducing blood lipids [38], regulating cholesterol metabolism [39], anti-inflammatory [40], improving endothelial cell dysfunction [41] .

Serum medicinal chemistry has become one of the main methods for studying the basis of pharmacodynamic substances of traditional Chinese medicine (TCM), and the identification of blood components through serum medicinal chemistry can be regarded as the main material basis for the effect of traditional Chinese medicine [42]. We used UHPLC-QE-MS to analyze the blood components of ASHP on rat drug-containing serum, and after comparing the obtained blood compounds with the database, two compounds were analyzed, namely, calycosin (PubChem CID: 5280448) and isorhamnetin (PubChem CID: 5281654). These two compounds, both of which belong to the flavonoid family, may be the most important key components of ASHP for the treatment of CHD. Flavonoids have been shown to reduce CVD mortality risk [43]. Calycosin are flavonoids derived from astragalus that have been shown to have antioxidant and anti-inflammatory activities. The study shows that calycosin promoted autophagy to prevent AS and improve plaque stability. By promoting autophagy, calycosin reduced inflammation, apoptosis, and foam cell formation. A previous study showed that calycosin's inhibitory effects on AS were mechanistically achieved by improving autophagy through modification of the KLF2-MLKL signaling pathway [44]. Isorhamnetin, a 3'-methoxyflavonol, has been reported in existing studies for its anti-atherosclerotic effects. Isorhamnetin prevented the growth of AS plaque in ApoE$^{-/-}$ mice by activating PI3K/AKT and inducing HO-1 [45]. The findings showed that salidroside, isorhamnetin, and both of them together suppressed the RhoA/ROCK II pathway. As a result, the inflammatory response under UII-induced circumstances was decreased, which attenuated the atherosclerotic process and provided cardioprotection [46]. Lysosomal dysfunction in macrophages has been linked to atherosclerosis development, isorhamnetin enhances lysosomal proteolysis in murine macrophages [47].

The most significant top 10 hub genes were obtained using the degree algorithm in the cytoHubba plugin, respectively *IL6, AKT1, IL1B, TP53, VEGFA, PTGS2, MMP9, CCL2, CXCL8*, and *EGF*. In the cardiovascular system, several cell types respond to inflammation, angiotensin II, oxidative stress, and vascular injury by producing IL-6. It has long been demonstrated that high levels of hsCRP and IL-6 indicate poor prognosis in both acute coronary ischemia and chronic secondary prevention [48]. Studies have confirmed that tocilizumab (an antibody to IL-6R) achieves an anti-atherosclerotic effect through endothelial dysfunction [49]. AKT1 plays a crucial role in the progression and development of AS as a crucial node in the PI3K/Akt/mTOR signaling pathway. The survival, proliferation, and migration of macrophages are all influenced by the PI3K/Akt pathway, which may have an effect on atherosclerosis progression [50]. MiR-155-5p performs a variety of biological cellular tasks in a wide range of pathologies, such as cardiovascular disease. By controlling AKT1, miR-155-5p inhibits the growth, movement, and invasion of VSMCs and HUVECs [51]. IL-1β and other members of the IL-1 family of cytokines are significant vascular and systemic inflammatory mediators that aid in the development of AS [52]. Clinical studies of CANTOS have confirmed that the reduction of inflammation in IL-1β inhibitor canakinumab significantly reduces the risk of previous myocardial infarction (MI) and residual inflammation [53]. Macrophages play an important role in the development of AS plaques. In early lipid infiltration, macrophages can form macrophage foam cells by ingesting oxidized LDL, one of the most fundamental features of early AS. The chemokine CCL2 expressed by macrophages promotes macrophage proliferation and migration through interaction with monocytes receptors, and participates in the occurrence and progression of AS plaques [54].

The metascape database was used to enrich GO and KEGG pathways for the common targets of ASHP and CHD. The results showed that the main signaling pathways included fluid shear stress and atherosclerosis, IL-17 signaling pathway, HIF-1 signaling pathway, NF-kappa B signaling pathway, and necroptosis. At the branches and curves of the arterial tree, where the blood flow pattern is disrupted, atherosclerosis develops preferentially. Studies have shown that shear stress in atherosclerosis regulates endothelial cell function through the SR-B1-eNOS signaling pathway [55]. By causing endothelial cell mechanotransduction and by regulating the near-wall transport pathways involved in atherosclerosis, wall shear stress (WSS) has an impact on coronary artery atherosclerosis [56]. IL-17/IL-17R signaling modality plays an important role in the pathogenesis of CAD. Li *et al.* [57] reported that hyperglycemia may aggravate coronary atherosclerosis by triggering TBK1-HIF-1-mediated IL-17/IL-10 signaling. Proinflammatory cytokines, chemokines, and matrix metalloproteinases produced by the IL-17 cytokine family play crucial roles in the development of inflammation. Kido *et al.* [58] reported that HIF-1α was involved in myocardial remodeling and peri-infarct vascularization. The serum hypoxia-inducible factor (HIF)-1α level was increased in the micro vessels after ischemia in all acute myocardial infarction (AMI) groups, while inhibition of HIF-1α decreased the angiogenic response *in vitro*, indicating that HIF-1α promoted inflammation and nuclear-factor kappa-

beta (NF-κB) played a key role in the development of atherosclerosis and CAD [59]. TLR4/MyD88/NF-κB signaling plays an important role in the development of coronary micro-embolism and myocardial inflammation. After coronary microembolization, TLR4/MyD88/NF-κB signaling contributes to the inflammatory response of the myocardium by activating the NLRP3 inflammasome, triggering the inflammatory cascade, and exacerbating myocardial damage [60]. One of the initial steps in the onset of atherosclerosis is the activation of ECs by pro-inflammatory chemicals and pathways. ECs' inflammatory response was suppressed by KLF14, suggesting that the protective effect was caused via transcriptional suppression of the NF-κB signaling pathway [61].

Cell death plays an irreplaceable role in the growth and development of the organism and other physiological functions. Programmed cell death includes apoptosis, necroptosis, proptosis, ferroptosis, and autophagy. Non-programmed death mainly includes necrosis. Proptosis is a recently identified caspase-dependent programmed cell death, which occurs in response to inflammation. The classical proptosis pathway is a Caspase-1-dependent pathway. A recent study found that apoptosis, necroptosis, and scorch death were closely associated with each other and cross-regulated by each other [62].

Necrotrophic signals can lead to IL-1β maturation and release via activation of the RIPK3-MLKL-NLRP3-Caspase-1 axis. In addition, MLKL-induced membrane damage leads to potassium efflux that activates the NLRP3 inflammasome, resulting in IL-1β driven inflammation [63]. As we have demonstrated using KEGG mapping color, MLKL activation of the NLRP3 inflammasome pathway can be seen in the pathway of necroptosis. Through the enormous production of pro-inflammatory cytokines like IL-1$\beta$and IL-18 and the death of several cell types, such as ECs, macrophages, and smooth muscle cells (SMCs), proptosis exacerbates plaque instability, leading to plaque rupture and thrombosis, ultimately leading to acute cardiovascular events. It is thought that systemic and local inflammation plays a key role in the transition from stable CAD to plaque instability and rupture. Some studies [64] found that aortic NLRP3 expression was highly correlated with the severity of coronary atherosclerosis. The study sought to ascertain the expression of NLRP3 inflammasome in peripheral blood monocytes (PBMCs) of patients with acute myocardial infarction and stable angina pectoris. It was found [65] that when NLRP3 inflammasome was expressed in peripheral blood monocytes (PBMCs), the level of IL-1 and IL-18 was elevated in both stable angina pectoris (SAP) and AMI groups as compared with that in the control group. Endothelial dysfunction is a marker and predictor of cardiovascular disease or adverse cardiovascular events such as CHD, diabetes and hypertension. Activation of NLRP3 inflammasome was found to be involved in endothelial inflammation, endothelial cell barrier dysfunction, and aging [66]. According to the mechanism of NLRP3 activation, blocking NLRP3 inflammasome activation may help minimize CHD damage caused by the sterile inflammatory response. By stifling early inflammatory responses after myocardial infarction, MCC950, a selective NLRP3 inhibitor, reduced fibrosis and enhanced the heart function in a mouse mode [67]. Multiple clinical research trials have also shown that drugs targeting NLRP3 inflammasome and molecules downstream of the pathway attenuate cardiovascular diseases such as CHD. Clinical trials such as LoDoCo, CANTOS and COLCOT showed that targeting inflammatory pathways connected to the NLRP3 inflammasome in patients with existing CAD helped prevent the occurrence of further cardiovascular events. Canakinumab is a human monoclonal antibody that targets IL-1β. CANTOS clinical trial [53] showed that recurrence of cardiovascular events was reduced considerably without affecting the LDL level after administration of 150mg canakinumab as compared with the placebo group. Astragalus and Astragalus IV, which is the main component of Astragalus , work by antagonizing the NLRP3 inflammasome-mediated apoptosis pathway, and have been reported in cerebral IR injury [68], lung injury [69], myocardial fibrosis and myocardial remodeling [70]. The action of Safflower on the NLRP3 inflammasome pathway has been studied in diseases such as atherosclerosis [16], myocardial IR [71], and depression [71], however, the application of ASHP in CHD and whether it plays a role in the apoptosis pathway mediated by NLRP3 inflammasomes are currently less studied.

We selected the core components in the ASHP and the key molecules of the signaling pathway mediated by NLRP3 inflammasomes, and the results showed that quercetin, kaempferol and apigenin can have good docking thermal energy with NLRP3 and caspase-1. We then validated it using vivo experiments. The results of the study showed that in the myocardial tissue of mice with CHD, inflammatory cells infiltrate, nuclear contraction, and the above situation was significantly improved after the intervention of ASHP. It was found in our study that the expression levels of NLRP3, caspase-1, GSDMD and IL-1β were significantly increased in the myocardial tissue of CHD mice as compared with those in the normal mice, suggesting that NLRP3 inflammasome-mediated apoptosis were involved in the progression of CHD (Fig. 15). The mechanism of ASHP acting on CHD shown in Fig. 15 may be that ASHP acts on the NLRP3 inflammasome-mediated signaling pathway, ultimately inhibiting the release of pyroptosis and inflammatory mediators, thereby treating CHD.

Based on the multiple network components between ASHP and CHD, we identified the main potential active components and action targets of ASHP and the related pathways, which may provide new ideas for further in-depth exploration of its action mechanism, though further experimental verification is required in the later stage.

However, the study still has some limitations. First, in

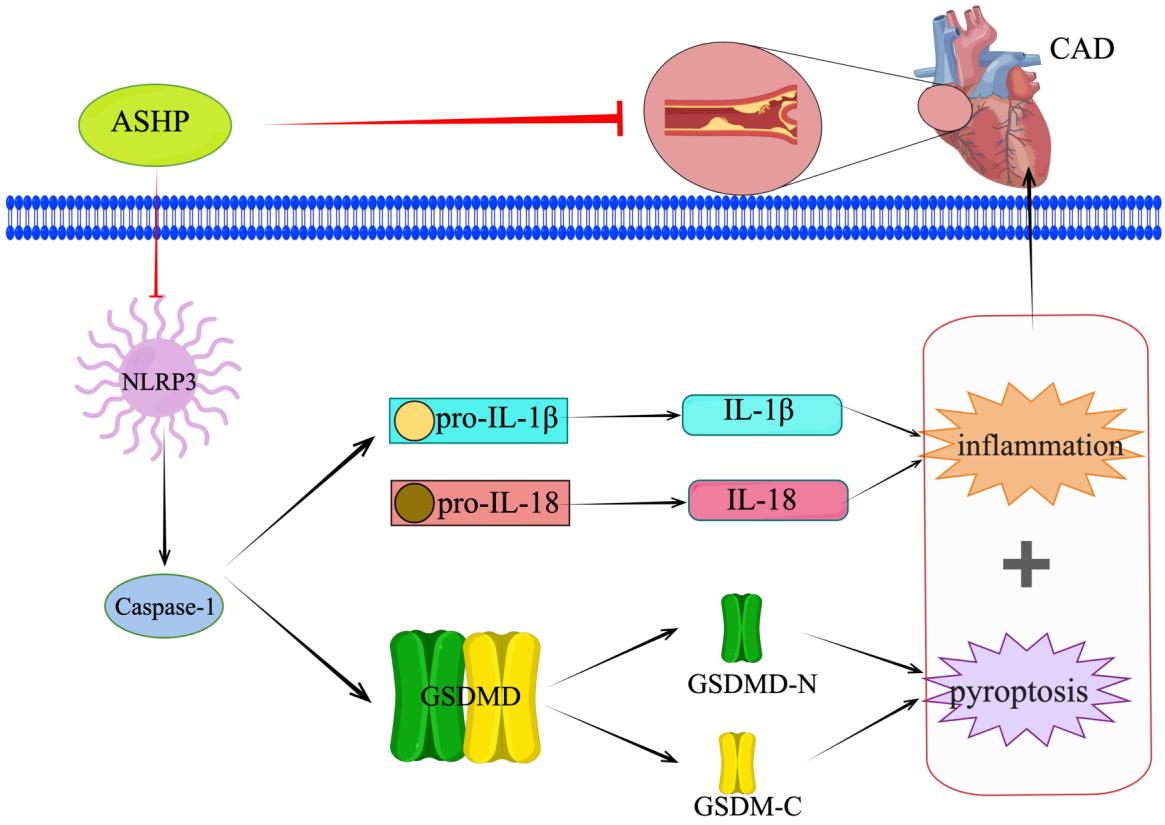

Fig. 15. ASHP treats CHD by inhibiting the NLRP3 inflammasome-mediated pyroptosis pathway.

the database search of drug ingredients and disease targets, only one was selected. In future research, it can be considered to search multiple drug ingredient target databases and disease target databases to make the study more comprehensive. Secondly, only the conventional dose of ASHP was selected in this study, and we all know that TCM has a positive dose-effect relationship, so it is necessary to increase the number of different doses to compare. At the same time, the ASHP should be compared with Astragalus and Safflower. Finally, in terms of experimental verification, only some indicators of *in vivo* experiments were selected for verification, and cell experiments needed to be added to further explore the mechanism.

5. Conclusions

A network pharmacology approach and molecular docking were used to investigate the effective components and key targets of ASHP in treating CHD. Multiple target genes and pathways were involved in the action of ASHP against CHD. Quercetin, kaempferol, apigenin, calycosin and isorhamnetin were shown to be the main effective compounds for the treatment of CHD, possibly exerting anti-CHD effects by inhibiting the NLRP3 inflammasome-mediated pyroptosis pathway. This study provides a more comprehensive understanding of the active components and targets of action of ASHP, which is beneficial for further optimization of CHD medication in the future.

Abbreviations

CHD, coronary heart disease; TCM, Traditional Chinese medicine; CVD, cardiovascular disease; CAD, coronary artery disease; NLRP3, NLR family pyrin domain containing 3; I/R, ischemia-reperfusion; OB, oral bioavailability; DL, drug-likeness; PPI, protein-protein interaction; BP, biological process; CC, cell composition; MF, molecular function; KEGG, Kyoto Encyclopedia of Genes and Genomes; HQ-HH, Huangqi-Honghua, Astragalus-Safflower; ASHP, Astragalus-Safflower herb pair; Ultrahigh-performance liquid chromatography coupled with Q-Exactive MS/MS, UPLC-QE-MS/MS; ECs, endothelial cells; LPS, lipopolysaccharide; HUVECs, human umbilical vein endothelial cells; SRA, Scavenger receptor A; KLF4, krüppel-like factor 4; PBS, phosphate-buffered saline; ox-LDL, oxidized low density lipoprotein; HFD, High-fat diet; AMI, acute myocardial infarction; SAP, stable angina pectoris; PBMCs, peripheral blood monocytes; SMCs, smooth muscle cells.

Availability of Data and Materials

Data are all contained within the paper and supplementary materials.

Author Contributions

YY is responsible for the drafting of the manuscript and the theoretical part of Traditional Chinese Medicine. HL is responsible for animal experiments and experimental data statistics. QM is responsible for the figures and grammar revision of the article. YY and HL have contributed equally to this work. Editorial modifications to the work were made by all writers. All the authors had read and approved the final manuscript. All authors have participated sufficiently in the work and agreed to be accountable for all aspects of the work.

Ethics Approval and Consent to Participate

The Institutional Animal Care and Use Committee of Hainan Medical University approved all animal experimentation techniques (Number: HYLL-2021-140). The animal experiment followed Guidelines for Ethical Review of the Welfare of Laboratory Animals in the People's Republic of China [GB/T 35892-2018].

Acknowledgment

The authors thank Science Experiment Center and Clinical Skills Experimental Teaching Center of Hainan Medical University gave support to the lab research.

Funding

This study was supported by the Open Project Fund of Hainan Provincial Key Laboratory of Tropical Brain Research and Transformation (JCKF2021001); The Natural Science Foundation of Hainan Province Youth Project (No.821QN401); Hainan Province Health and Health Industry Research Project (No.21A200344); The First Affiliated Hospital of Hainan Medical University Youth Incubation Fund (No. HYYHYPY202006).

Conflict of Interest

The authors declare no conflict of interest.

Supplementary Material

Supplementary material associated with this article can be found, in the online version, at https://doi.org/10.31083/j.fbl2805094.

References

[1] Roth GA, Mensah GA, Johnson CO, Addolorato G, Ammirati E, Baddour LM, *et al*. Global Burden of Cardiovascular Diseases and Risk Factors, 1990-2019: Update From the GBD 2019 Study. Journal of the American College of Cardiology. 2020; 76: 2982–3021.

[2] Zhao D, Liu J, Wang M, Zhang X, Zhou M. Epidemiology of cardiovascular disease in China: current features and implications. Nature Reviews Cardiology. 2019; 16: 203–212.

[3] Stone NJ. Statins in Secondary Prevention: Intensity Matters. Journal of the American College of Cardiology. 2017; 69: 2707–2709.

[4] Guo Y, Wei J. Clinical outcomes of various continued antiplatelet therapies in patients who were administered DAPT following the implantation of drug-eluting stents and developed gastrointestinal hemorrhage. Experimental and Therapeutic Medicine. 2016; 12: 1125–1129.

[5] Baginsky P. Should we treat all patients with coronary heart disease or the equivalent with statins? Current Atherosclerosis Reports. 2009; 11: 28–35.

[6] Liang B, Zhang XX, Li R, Zhu YC, Tian XJ, Gu N. Guanxin V alleviates acute myocardial infarction by restraining oxidative stress damage, apoptosis, and fibrosis through the TGF-β1 signalling pathway. Phytomedicine: International Journal of Phytotherapy and Phytopharmacology. 2022; 100: 154077.

[7] Liang B, Qu Y, Zhao QF, Gu N. Guanxin V for coronary artery disease: A retrospective study. Biomedicine & Pharmacotherapy. 2020; 128: 110280.

[8] Cao J, Chen Z, Zhu Y, Li Y, Guo C, Gao K, *et al*. Huangqi-Honghua combination and its main components ameliorate cerebral infarction with Qi deficiency and blood stasis syndrome by antioxidant action in rats. Journal of Ethnopharmacology. 2014; 155: 1053–1060.

[9] Zheng Y, Ren W, Zhang L, Zhang Y, Liu D, Liu Y. A Review of the Pharmacological Action of Astragalus Polysaccharide. Frontiers in Pharmacology. 2020; 11: 349.

[10] Lin XP, Cui HJ, Yang AL, Luo JK, Tang T. Astragaloside IV Improves Vasodilatation Function by Regulating the PI3K/Akt/eNOS Signaling Pathway in Rat Aorta Endothelial Cells. Journal of Vascular Research. 2018; 55: 169–176.

[11] Ma C, Xia R, Yang S, Liu L, Zhang J, Feng K, *et al*. Formononetin attenuates atherosclerosis via regulating interaction between KLF4 and SRA in apoE$^{-/-}$ mice. Theranostics. 2020; 10: 1090–1106.

[12] Su Y, Yin X, Huang X, Guo Q, Ma M, Guo L. The BCL2/BAX/ROS pathway is involved in the inhibitory effect of astragaloside IV on pyroptosis in human umbilical vein endothelial cells. Pharmaceutical Biology. 2022; 60: 1812–1818.

[13] Meng Q, Liu H, Wu H, Shun D, Tang C, Fu X, *et al*. A Network Pharmacology Study to Explore the Underlying Mechanism of Safflower (*Carthamus tinctorius L.*) in the Treatment of Coronary Heart Disease. Evidence-based Complementary and Alternative Medicine: ECAM. 2022; 2022: 3242015.

[14] Zhou D, Qu Z, Wang H, Su Y, Wang Y, Zhang W, *et al*. The effect of hydroxy safflower yellow A on coronary heart disease through Bcl-2/Bax and PPAR-γ. Experimental and Therapeutic Medicine. 2018; 15: 520–526.

[15] Li LM, Fu JH, Guo H, Han X, Li L, Xin GJ, *et al*. Protective effect of safflower yellow injection against rat MIRI by TLR-NF-κB inflammatory pathway. Zhongguo Zhong Yao Za Zhi. 2019; 44: 2566–2571. (In Chinese)

[16] Xue X, Deng Y, Wang J, Zhou M, Liao L, Wang C, *et al*. Hydroxysafflor yellow A, a natural compound from Carthamus tinctorius L with good effect of alleviating atherosclerosis. Phytomedicine: International Journal of Phytotherapy and Phytopharmacology. 2021; 91: 153694.

[17] Zhao X, He Y, Zhang Y, Wan H, Wan H, Yang J. Inhibition of Oxidative Stress: An Important Molecular Mechanism of Chinese Herbal Medicine (Astragalus membranaceus, Carthamus tinctorius L., Radix Salvia Miltiorrhizae, etc.) in the Treatment of Ischemic Stroke by Regulating the Antioxidant System. Oxidative Medicine and Cellular Longevity. 2022; 2022: 1425369.

[18] Chen Q, Wan J, Zhang Y, He Y, Bao Y, Yu L, *et al*. Pharmacokinetic-pharmacodynamic modeling analysis for hydroxysafflor yellow A-calycosin in compatibility in normal and cerebral ischemic rats: A comparative study. Biomedicine & Pharmacotherapy. 2022; 150: 112950.

[19] Liang B, Liang Y, Li R, Zhang H, Gu N. Integrating systematic pharmacology-based strategy and experimental validation to ex-

plore the synergistic pharmacological mechanisms of Guanxin V in treating ventricular remodeling. Bioorganic Chemistry. 2021; 115: 105187.

[20] Szklarczyk D, Gable AL, Nastou KC, Lyon D, Kirsch R, Pyysalo S, *et al*. The STRING database in 2021: customizable protein-protein networks, and functional characterization of user-uploaded gene/measurement sets. Nucleic Acids Research. 2021; 49: D605–D612.

[21] Piñero J, Bravo À, Queralt-Rosinach N, Gutiérrez-Sacristán A, Deu-Pons J, Centeno E, *et al*. DisGeNET: a comprehensive platform integrating information on human disease-associated genes and variants. Nucleic Acids Research. 2017; 45: D833–D839.

[22] Di H, Liu H, Xu S, Yi N, Wei G. Network Pharmacology and Experimental Validation to Explore the Molecular Mechanisms of Compound Huangbai Liquid for the Treatment of Acne. Drug Design, Development and Therapy. 2023; 17: 39–53.

[23] Doncheva NT, Morris JH, Gorodkin J, Jensen LJ. Cytoscape StringApp: Network Analysis and Visualization of Proteomics Data. Journal of Proteome Research. 2019; 18: 623–632.

[24] Zhou Y, Zhou B, Pache L, Chang M, Khodabakhshi AH, Tanaseichuk O, *et al*. Metascape provides a biologist-oriented resource for the analysis of systems-level datasets. Nature Communications. 2019; 10: 1523.

[25] Kim S, Chen J, Cheng T, Gindulyte A, He J, He S, *et al*. PubChem in 2021: new data content and improved web interfaces. Nucleic Acids Research. 2021; 49: D1388–D1395.

[26] Huang X, Chu Y, Ren H, Pang X. Antioxidation Function of EGCG by Activating Nrf2/HO-1 Pathway in Mice with Coronary Heart Disease. Contrast Media & Molecular Imaging. 2022; 2022: 8639139.

[27] Li S, Zhang B. Traditional Chinese medicine network pharmacology: theory, methodology and application. Chinese Journal of Natural Medicines. 2013; 11: 110–120.

[28] González-Cofrade L, Cuadrado I, Amesty Á, Estévez-Braun A, de Las Heras B, Hortelano S. Dehydroisohispanolone as a Promising NLRP3 Inhibitor Agent: Bioevaluation and Molecular Docking. Pharmaceuticals (Basel, Switzerland). 2022; 15: 825.

[29] Matyszewski M, Zheng W, Lueck J, Antiochos B, Egelman EH, Sohn J. Cryo-EM structure of the NLRC4^{CARD} filament provides insights into how symmetric and asymmetric supramolecular structures drive inflammasome assembly. The Journal of Biological Chemistry. 2018; 293: 20240–20248.

[30] Sharma R, Jadhav M, Choudhary N, Kumar A, Rauf A, Gundamaraju R, *et al*. Deciphering the impact and mechanism of Trikatu, a spices-based formulation on alcoholic liver disease employing network pharmacology analysis and *in vivo* validation. Frontiers in Nutrition. 2022; 9: 1063118.

[31] Choudhary N, Singh V. A census of P. longum's phytochemicals and their network pharmacological evaluation for identifying novel drug-like molecules against various diseases, with a special focus on neurological disorders. PLoS ONE. 2018; 13: e0191006.

[32] Sharma R, Singla RK, Banerjee S, Sinha B, Shen B, Sharma R. Role of Shankhpushpi (Convolvulus pluricaulis) in neurological disorders: An umbrella review covering evidence from ethnopharmacology to clinical studies. Neuroscience and Biobehavioral Reviews. 2022; 140: 104795.

[33] Chen WJ, Cheng Y, Li W, Dong XK, Wei JL, Yang CH, *et al*. Quercetin Attenuates Cardiac Hypertrophy by Inhibiting Mitochondrial Dysfunction Through SIRT3/PARP-1 Pathway. Frontiers in Pharmacology. 2021; 12: 739615.

[34] Yu S, Kim SR, Jiang K, Ogrodnik M, Zhu XY, Ferguson CM, *et al*. Quercetin Reverses Cardiac Systolic Dysfunction in Mice Fed with a High-Fat Diet: Role of Angiogenesis. Oxidative Medicine and Cellular Longevity. 2021; 2021: 8875729.

[35] Nie J, Zhang L, Zhao G, Du X. Quercetin reduces atherosclerotic lesions by altering the gut microbiota and reducing atherogenic lipid metabolites. Journal of Applied Microbiology. 2019; 127: 1824–1834.

[36] Xiao L, Liu L, Guo X, Zhang S, Wang J, Zhou F, *et al*. Quercetin attenuates high fat diet-induced atherosclerosis in apolipoprotein E knockout mice: A critical role of NADPH oxidase. Food and Chemical Toxicology: an International Journal Published for the British Industrial Biological Research Association. 2017; 105: 22–33.

[37] Feng H, Cao J, Zhang G, Wang Y. Kaempferol Attenuates Cardiac Hypertrophy via Regulation of ASK1/MAPK Signaling Pathway and Oxidative Stress. Planta Medica. 2017; 83: 837–845.

[38] Xu Q, Li YC, Du C, Wang LN, Xiao YH. Effects of Apigenin on the Expression of LOX-1, Bcl-2, and Bax in Hyperlipidemia Rats. Chemistry & Biodiversity. 2021; 18: e2100049.

[39] Zhang K, Song W, Li D, Jin X. Apigenin in the regulation of cholesterol metabolism and protection of blood vessels. Experimental and Therapeutic Medicine. 2017; 13: 1719–1724.

[40] Kumar KS, Sabu V, Sindhu G, Rauf AA, Helen A. Isolation, identification and characterization of apigenin from Justicia gendarussa and its anti-inflammatory activity. International Immunopharmacology. 2018; 59: 157–167.

[41] Lamb NJ, Gizard F. Dietary Apigenin in the Prevention of Endothelial Cell Dysfunction. Journal of Cardiovascular Pharmacology. 2019; 74: 513–515.

[42] Ma FX, Xue PF, Wang YY, Wang YN, Xue SY. Research progress of serum pharmacochemistry of traditional Chinese medicine. Zhongguo Zhong Yao Za Zhi. 2017; 42: 1265–1270. (In Chinese)

[43] Ma L, Liu G, Ding M, Zong G, Hu FB, Willett WC, *et al*. Isoflavone Intake and the Risk of Coronary Heart Disease in US Men and Women: Results From 3 Prospective Cohort Studies. Circulation. 2020; 141: 1127–1137.

[44] Ma C, Wu H, Yang G, Xiang J, Feng K, Zhang J, *et al*. Calycosin ameliorates atherosclerosis by enhancing autophagy via regulating the interaction between KLF2 and MLKL in apolipoprotein E gene-deleted mice. British Journal of Pharmacology. 2022; 179: 252–269.

[45] Luo Y, Sun G, Dong X, Wang M, Qin M, Yu Y, *et al*. Isorhamnetin attenuates atherosclerosis by inhibiting macrophage apoptosis via PI3K/AKT activation and HO-1 induction. PLoS ONE. 2015; 10: e0120259.

[46] Wang C, Nan X, Pei S, Zhao Y, Wang X, Ma S, *et al*. Salidroside and isorhamnetin attenuate urotensin II-induced inflammatory response *in vivo* and *in vitro*: Involvement in regulating the RhoA/ROCK II pathway. Oncology Letters. 2021; 21: 292.

[47] Sakai M, Ohnishi K, Masuda M, Ohminami H, Yamanaka-Okumura H, Hara T, *et al*. Isorhamnetin, a 3'-methoxylated flavonol, enhances the lysosomal proteolysis in J774.1 murine macrophages in a TFEB-independent manner. Bioscience, Biotechnology, and Biochemistry. 2020; 84: 1221–1231.

[48] Held C, White HD, Stewart RAH, Budaj A, Cannon CP, Hochman JS, *et al*. Inflammatory Biomarkers Interleukin-6 and C-Reactive Protein and Outcomes in Stable Coronary Heart Disease: Experiences From the STABILITY (Stabilization of Atherosclerotic Plaque by Initiation of Darapladib Therapy) Trial. Journal of the American Heart Association. 2017; 6: e005077.

[49] Hafiane A, Daskalopoulou SS. Targeting the residual cardiovascular risk by specific anti-inflammatory interventions as a therapeutic strategy in atherosclerosis. Pharmacological Research. 2022; 178: 106157.

[50] Linton MF, Moslehi JJ, Babaev VR. Akt Signaling in Macrophage Polarization, Survival, and Atherosclerosis. Inter-

national Journal of Molecular Sciences. 2019; 20: 2703.
[51] Chen L, Zheng SY, Yang CQ, Ma BM, Jiang D. MiR-155-5p inhibits the proliferation and migration of VSMCs and HUVECs in atherosclerosis by targeting AKT1. European Review for Medical and Pharmacological Sciences. 2019; 23: 2223–2233.
[52] Grebe A, Hoss F, Latz E. NLRP3 Inflammasome and the IL-1 Pathway in Atherosclerosis. Circulation Research. 2018; 122: 1722–1740.
[53] Ridker PM, Everett BM, Thuren T, MacFadyen JG, Chang WH, Ballantyne C, *et al*. Antiinflammatory Therapy with Canakinumab for Atherosclerotic Disease. The New England Journal of Medicine. 2017; 377: 1119–1131.
[54] Tabas I, Bornfeldt KE. Macrophage Phenotype and Function in Different Stages of Atherosclerosis. Circulation Research. 2016; 118: 653–667.
[55] Zhang Y, Liao B, Li M, Cheng M, Fu Y, Liu Q, *et al*. Shear stress regulates endothelial cell function through SRB1-eNOS signaling pathway. Cardiovascular Therapeutics. 2016; 34: 308–313.
[56] Mahmoudi M, Farghadan A, McConnell DR, Barker AJ, Wentzel JJ, Budoff MJ, *et al*. The Story of Wall Shear Stress in Coronary Artery Atherosclerosis: Biochemical Transport and Mechanotransduction. Journal of Biomechanical Engineering. 2021; 143: 041002.
[57] Li Q, Liu Y, Xia X, Sun H, Gao J, Ren Q, *et al*. Activation of macrophage TBK1-HIF-1α-mediated IL-17/IL-10 signaling by hyperglycemia aggravates the complexity of coronary atherosclerosis: An *in vivo* and *in vitro* study. FASEB Journal: Official Publication of the Federation of American Societies for Experimental Biology. 2021; 35: e21609.
[58] Kido M, Du L, Sullivan CC, Li X, Deutsch R, Jamieson SW, *et al*. Hypoxia-inducible factor 1-alpha reduces infarction and attenuates progression of cardiac dysfunction after myocardial infarction in the mouse. Journal of the American College of Cardiology. 2005; 46: 2116–2124.
[59] Ríos-Navarro C, Hueso L, Miñana G, Núñez J, Ruiz-Saurí A, Sanz MJ, *et al*. Coronary Serum Obtained After Myocardial Infarction Induces Angiogenesis and Microvascular Obstruction Repair. Role of Hypoxia-inducible Factor-1A. Revista Espanola De Cardiologia (English Ed.). 2018; 71: 440–449.
[60] Su Q, Li L, Sun Y, Yang H, Ye Z, Zhao J. Effects of the TLR4/Myd88/NF-κB Signaling Pathway on NLRP3 Inflammasome in Coronary Microembolization-Induced Myocardial Injury. Cellular Physiology and Biochemistry: International Journal of Experimental Cellular Physiology, Biochemistry, and Pharmacology. 2018; 47: 1497–1508.
[61] Hu W, Lu H, Zhang J, Fan Y, Chang Z, Liang W, *et al*. Krüppel-like factor 14, a coronary artery disease associated transcription factor, inhibits endothelial inflammation via NF-κB signaling pathway. Atherosclerosis. 2018; 278: 39–48.
[62] Bertheloot D, Latz E, Franklin BS. Necroptosis, pyroptosis and apoptosis: an intricate game of cell death. Cellular & Molecular Immunology. 2021; 18: 1106–1121.
[63] Lawlor KE, Khan N, Mildenhall A, Gerlic M, Croker BA, D'Cruz AA, *et al*. RIPK3 promotes cell death and NLRP3 inflammasome activation in the absence of MLKL. Nature Communications. 2015; 6: 6282.
[64] Zheng F, Xing S, Gong Z, Xing Q. NLRP3 inflammasomes show high expression in aorta of patients with atherosclerosis. Heart, Lung & Circulation. 2013; 22: 746–750.
[65] Zhu J, Wu S, Hu S, Li H, Li M, Geng X, *et al*. NLRP3 inflammasome expression in peripheral blood monocytes of coronary heart disease patients and its modulation by rosuvastatin. Molecular Medicine Reports. 2019; 20: 1826–1836.
[66] Bai B, Yang Y, Wang Q, Li M, Tian C, Liu Y, *et al*. NLRP3 inflammasome in endothelial dysfunction. Cell Death & Disease. 2020; 11: 776.
[67] Gao R, Shi H, Chang S, Gao Y, Li X, Lv C, *et al*. The selective NLRP3-inflammasome inhibitor MCC950 reduces myocardial fibrosis and improves cardiac remodeling in a mouse model of myocardial infarction. International Immunopharmacology. 2019; 74: 105575.
[68] Xiao L, Dai Z, Tang W, Liu C, Tang B. Astragaloside IV Alleviates Cerebral Ischemia-Reperfusion Injury through NLRP3 Inflammasome-Mediated Pyroptosis Inhibition via Activating Nrf2. Oxidative Medicine and Cellular Longevity. 2021; 2021: 9925561.
[69] Chen G, Hou Y, Li X, Pan R, Zhao D. Sepsis-induced acute lung injury in young rats is relieved by calycosin through inactivating the HMGB1/MyD88/NF-κB pathway and NLRP3 inflammasome. International Immunopharmacology. 2021; 96: 107623.
[70] Zhang X, Qu H, Yang T, Liu Q, Zhou H. Astragaloside IV attenuate MI-induced myocardial fibrosis and cardiac remodeling by inhibiting ROS/caspase-1/GSDMD signaling pathway. Cell Cycle (Georgetown, Tex.). 2022; 21: 2309–2322.
[71] Ye J, Lu S, Wang M, Ge W, Liu H, Qi Y, *et al*. Hydroxysafflor Yellow A Protects Against Myocardial Ischemia/Reperfusion Injury *via* Suppressing NLRP3 Inflammasome and Activating Autophagy. Frontiers in Pharmacology. 2020; 11: 1170.